

# Full Flight-Envelope Simulation and Piloted Fidelity Assessment of a Business Jet Using a Model Stitching Architecture

Eric L. Tobias\*

*San Jose State University Foundation, Moffett Field, CA*

Mark B. Tischler†

*U.S. Army Aviation Development Directorate – AFDD, Moffett Field, CA*

Tom Berger‡

*University Affiliated Research Center, Moffett Field, CA*

Steven G. Hagerott§

*Cessna Aircraft Company, Wichita, KS*

This paper presents the development and piloted assessment of a full flight-envelope simulation model of a light business jet using a model stitching architecture. Individual state-space models and trim data for discrete flight conditions were combined to produce a continuous simulation model, which was integrated into a fixed-base simulation facility. Back-to-back flight/simulation piloted evaluations of a similar light business jet in flight and the stitched model in simulation were performed to assess the fidelity of the stitched model. Overall pilot impressions were that the stitched simulation model was representative of the actual aircraft. Simulation Fidelity Ratings were given to quantify simulation fidelity for each of the evaluated qualitative tasks, in which mostly Fidelity Level 1 ratings were assigned, suggesting full transfer of training for those tasks. Guidance on flight testing for the development of fixed-wing aircraft stitched models is provided.

## Nomenclature

|                          |   |
|--------------------------|---|
| $A, B, C, D$             | State-space matrix representation of dynamic system model                                 |
| $F$                      | External force vector [lb]  |
| $g$                      | Acceleration due to gravity [ft/sec <sup>2</sup> ]  |
| $I$                      | Inertia tensor  |
| $I_{xx}, I_{yy}, I_{zz}$ | Moments of inertia (roll, pitch, yaw) [slug-ft <sup>2</sup> ]                             |
| $I_{xz}$                 | Product of inertia [slug-ft <sup>2</sup> ]  |
| $L, M, N$                | External moments about the aircraft CG (roll, pitch, yaw) [lb-ft]                         |
| $M$                      | External moment vector [lb-ft]  |
| $\mathcal{M}$            | Mass matrix comprised of aircraft mass and inertia tensor                                 |
| $m$                      | Aircraft mass [slug]  |
| $P, Q, R$                | Fuselage total (absolute) angular rates (roll, pitch, yaw) [rad/sec]                      |
| $s$                      | Laplace variable  |
| $U$                      | Total (absolute) vector of controls   |
| $u$                      | Perturbation vector of controls   |
| $U, V, W$                | Body-axis total (absolute) velocity components (longitudinal, lateral, vertical) [ft/sec] |
| $u, v, w$                | Body-axis perturbation velocity components (longitudinal, lateral, vertical) [ft/sec]     |

\*Research Associate, Flight Control Technology, Member AIAA.

†Flight Control Technology Group Leader, Senior Scientist, U.S. Army Aviation Development Directorate – AFDD, Associate Fellow AIAA.

‡Research Engineer, Flight Control Technology, Senior Member AIAA.

§Senior Engineer Specialist, Aerosciences, Cessna Aircraft Company, Senior Member AIAA.

Approved for public release; distribution is unlimited.

|  |   |
|--|---|
| $\mathbf{X}$                             | Total (absolute) vector of states   |
| $\mathbf{x}$                             | Perturbation vector of states   |
| $X, Y, Z$                                | External forces on the aircraft CG (longitudinal, lateral, vertical) [lb] |
| $\mathbf{Y}$                             | Total (absolute) vector of outputs  |
| $\mathbf{y}$                             | Perturbation vector of outputs  |
| $\alpha$                                 | Angle of attack [rad]   |
| $\beta$                                  | Angle of sideslip [rad]   |
| $\Delta$                                 | Perturbation  |
| $\delta_a, \delta_e, \delta_r, \delta_t$ | Control inputs (aileron, elevator, rudder, thrust) [rad, rad, rad, lb]    |
| $\Phi, \Theta, \Psi$                     | Fuselage total (absolute) attitudes (roll, pitch, yaw) [rad]              |
| $\phi, \theta, \psi$                     | Fuselage perturbation attitudes (roll, pitch, yaw) [rad]                  |
| $\rho$                                   | Atmospheric air density [slug/ft <sup>3</sup> ]                           |
| AAA                                      | Advanced Aircraft Analysis software (DARcorporation)                      |
| CG                                       | Center of gravity   |
| DOF                                      | Degree(s) of freedom  |
| KCAS                                     | Knots calibrated airspeed   |
| KTAS                                     | Knots true airspeed   |
| <i>Subscript</i>                         |   |
| sim                                      | Simulation value  |
| 0  | Trim value  |

## I. Introduction

LINEAR state-space perturbation models, which represent the dynamic response of an aircraft for a discrete reference flight condition and configuration, are accurate within some limited range of the reference condition. These discrete point linear models, as derived from system identification from flight testing or a non-realtime model, for example, may be produced at suitable airspeed and altitude increments to construct a collection of discrete models to describe the aircraft dynamics at specific points over the desired flight envelope. These discrete models are suitable for point design of control systems and point handling qualities analyses; however, continuous simulation is desirable for full-mission piloted simulation.

*Model stitching* refers to the technique of combining or “stitching” together individual linear models and trim data for discrete flight conditions to produce a continuous, full flight-envelope simulation model.<sup>1</sup> In this technique, the stability and control derivatives and trim data for each discrete point model are stored in lookup tables as a function of key parameters such as airspeed and altitude. The look-up of trim and derivatives is combined with nonlinear equations of motion and nonlinear gravity force equations to produce a continuous, quasi-nonlinear, *stitched* simulation model.

The theoretical concept of the model stitching technique has been applied to develop a *model stitching simulation architecture*, which incorporates extrapolation methods for the simulation of off-nominal aircraft loading configurations, including variations in weight, inertia, and center of gravity, and utilizes an extrapolation method for altitude variation. These extrapolation methods allow for continuous simulation of aircraft loading changes due to fuel burn-off or jettisoning of external stores, for example. Also incorporated into the model stitching architecture are additional modeling components, including turbulence and a standard atmosphere model, as well as accommodations for user-specified modeling components, such as engine models and landing gear.

A state-of-the-art, full flight-envelope stitched simulation model of a light business jet, representative of the Cessna Citation CJ1, was developed using the model stitching architecture. Dimensional linear state-space models and trim data of the bare airframe were generated using nondimensional stability and control derivatives output from the Advanced Aircraft Analysis<sup>2</sup> (AAA) software utility for discrete flight conditions. Additional airframe-specific modeling elements, including flaps and spoilers, were incorporated into the CJ1 stitched model, making it ideal for realistic, full-mission piloted evaluations.

Primary objectives of the current study were to assess the qualitative fidelity of the CJ1 stitched model in piloted simulation and utilize the Simulation Fidelity Rating<sup>3</sup> (SFR) scale to quantify simulation fidelity for the selected evaluation tasks. Use of the SFR scale requires the pilots to first perform the given tasks in a representative aircraft in flight, thus a 2-hour flight evaluation was conducted in a light business jet similar to the CJ1. Tasks were then repeated in Cessna’s fixed-base simulator facility following the flight evaluation.

Comparative task performance and task strategy adaptation between flight and simulation were considered for each evaluated task, which translated to a Simulation Fidelity Rating. A secondary objective of this study was to determine the recommended number of discrete point models and trim data points necessary for extrapolation to accurately cover the full flight-envelope in the stitched model, while considering system identification flight test implications.

This paper first presents an overview of the model stitching technique and its implementation into a comprehensive model stitching simulation architecture. Specific application of the model stitching architecture for the development of a full flight-envelope stitched simulation model of a light business jet using discrete point models from AAA is discussed. Experiment setup, including verification of the piloted simulation environment and selection of qualitative evaluation tasks, is covered. Results of the piloted fidelity assessment, including SFRs and pilot impressions, are presented and discussed. Guidance on flight testing for the development of fixed-wing aircraft stitched models is provided. Lessons learned are discussed and overall conclusions determined from the experiment are stated.

## II. Model Stitching Simulation Architecture

The term *model stitching* refers to the technique of combining or “stitching” together a collection of linear state-space models for discrete flight conditions, with corresponding trim data, into one continuous, full-envelope flight-dynamics simulation model. In this technique, the stability and control derivatives and trim data for each discrete point model are stored in lookup tables as a function of key parameters such as airspeed, altitude, or aircraft configuration. This modeling technique is in the class of quasi-linear-parameter-varying (qLPV) models.<sup>4</sup> The resulting *stitched model* is time-varying and quasi-nonlinear in that the stability and control derivatives and trim data are scheduled, but nonlinear equations of motion and nonlinear gravity force equations are implemented. Essentially, the stitched model is a nonlinear flight-dynamics simulation model with linear, time-varying aerodynamics.

A comprehensive *model stitching simulation architecture* has been developed that is applicable to any generic flight vehicle, and allows for the inclusion of airframe-specific elements (e.g., spoilers, landing gear, etc.). Off-nominal aircraft loading configurations, including variations in weight, inertia, and center of gravity (CG) location, are accounted for by the model stitching architecture. This capability allows for real-time simulation of aircraft loading changes due to fuel burn-off or jettisoning of external stores, for example.

Closed-loop control system analysis and full flight-envelope piloted simulation of bare-airframe dynamics are key applications for a stitched model. Because of the continuous nature of the stitched model, a full mission consisting of takeoff, climb, cruise, and flight maneuvers, for example, can be executed in a continuous, real-time fashion. The incorporation of airframe-specific modeling elements such as landing gear, flaps, and spoilers, and atmospheric elements such as turbulence and steady wind into the stitched model adds fidelity and realism to the simulation environment.

Some background and previous work are mentioned in Section II.A. Basic theory and concepts of the model stitching technique, following closely those presented in Tischler,<sup>1</sup> are covered in Section II.B. Implementation of the theory into the model stitching simulation architecture is presented in Section II.C. Specific application of the model stitching architecture for the development of the CJ1 business jet stitched simulation model is presented in Section III.

### A. Background and Previous Work

The model stitching technique was first proposed by Aiken<sup>5</sup> and Tischler.<sup>6</sup> Tischler outlines the model stitching approach as applicable to a piloted V/STOL simulation, and covers key theoretical model stitching concepts including the implicit representation of speed perturbation derivatives, the balancing of gravity forces by the trim aerodynamic forces, the inclusion of nonlinear equations of motion, and data requirements for accurate simulation throughout the flight envelope.

Zivan and Tischler<sup>7</sup> built on this early work and produced a stitched model of the Bell 206 helicopter from a series of individual, flight-identified point models. Seven state-space point models, covering a flight envelope of hover through high-speed forward flight and two altitudes, were generated using frequency-domain system identification in CIPHER<sup>®</sup>. The stitched model was implemented in a simple, fixed-base simulator and evaluated by several pilots, all qualified in the 206. The evaluation procedure was based on the pilots rating the similarity between the model and the actual aircraft using a specialized rating scale. Evaluation

maneuvers included large and small amplitude doublets/steps, coordinated turns, and climbs/descents to cover most of the helicopter’s flight envelope. Overall pilot opinion was that the simulation was a good representation of the aircraft for all evaluated tasks.

In their development of a stitched simulation model of a tiltrotor, Lawrence et al.<sup>8</sup> employed the stitching technique in airspeed as well as in engine nacelle angle to develop a real-time simulation of a large civil tiltrotor at hover through low speed (up to 60 kn). This model has been used in several piloted studies of hover/low-speed handling-qualities requirements for large civil tiltrotor configurations. Another recent application is to the simulation of the unmanned K-MAX BURRO helicopter by Mansur et al.<sup>9</sup> Four identified state-space models (two at low altitude and two at high altitude) were shown to effectively cover the desired flight envelope. Evaluations of a full-envelope mission simulation validated that a broad spacing of identified point models was satisfactory.

## B. Basic Model Stitching Concepts

The key requirement for model stitching is a series of state-space models and associated trim data of the states and controls for several discrete flight conditions, or “anchor” points, covering a range of airspeed and perhaps altitude and aircraft configuration. The point models and trim data may be identified from flight testing or derived from a more complex, non-realtime model, for example.

The model stitching equations are formulated to accommodate simulation of any generic flight vehicle, in which dynamics and trim are likely dependent not only on total airspeed but also on body-axes velocity components, such as rotorcraft in sideward flight.<sup>1</sup> Hence, the model stitching technique is formulated in *body axes*, in which the interpolation of stability and control derivatives and trim data must be with respect to the individual body-axes airspeed components. The model stitching technique can be reformulated in other axis conventions, but it is demonstrated herein that simple transformation equations may be utilized to effectively transform stability-axes derivatives into body-axes derivatives for use in the model stitching simulation architecture.

Although model stitching may be performed as a function of multiple simultaneous interpolation (table lookup) dimensions, this overview of basic concepts will demonstrate model stitching in airspeed only. Conforming to the body-axes formulation, stability and control derivatives and trim data are interpolated based on the absolute  $x$ -body axis airspeed component  $U$ , not total airspeed  $V_{\text{tot}}$ .

Given a linear model of a specific aircraft configuration, the generalized state-space representation is utilized to give the appropriate perturbation dynamic response about a reference (anchor) flight condition with trim  $x$ -body axis airspeed  $U_0$ :

$$\dot{\mathbf{x}} = \mathbf{A}|_{U_0}\mathbf{x} + \mathbf{B}|_{U_0}\mathbf{u} \quad (1)$$

$$\mathbf{y} = \mathbf{C}|_{U_0}\mathbf{x} + \mathbf{D}|_{U_0}\mathbf{u} \quad (2)$$

which is expressed in terms of the stability and control derivatives for the reference flight condition, the perturbation state vector  $\mathbf{x}$ , and the perturbation control vector  $\mathbf{u}$ .

The state-space representation is then rewritten in terms of the vectors of total (absolute) values of states  $\mathbf{X}$ , controls  $\mathbf{U}$ , and outputs  $\mathbf{Y}$  rather than perturbation values, and at the instantaneous  $x$ -body axis airspeed  $U$  instead of reference trim  $x$ -body axis airspeed  $U_0$ . Vectors of trim states  $\mathbf{X}_0$  and trim controls  $\mathbf{U}_0$  are included forming a continuous, full flight-envelope simulation model by expressing the state-space equations as

$$\dot{\mathbf{X}} = \mathbf{A}|_U(\mathbf{X} - \mathbf{X}_0|_U) + \mathbf{B}|_U(\mathbf{U} - \mathbf{U}_0|_U) \quad (3)$$

$$\mathbf{Y} = \mathbf{C}|_U(\mathbf{X} - \mathbf{X}_0|_U) + \mathbf{D}|_U(\mathbf{U} - \mathbf{U}_0|_U) + \mathbf{Y}_0|_U \quad (4)$$

Trim states, controls, and stability/control derivatives are then all interpolated via table lookup based on the instantaneous  $x$ -body axis airspeed  $U$ , as denoted by  $|_U$ . As expected from Equations (3) and (4), at reference speed of  $U = U_0$ , the continuous simulation will trim ( $\dot{\mathbf{X}} = 0$ ) with model states, controls, and outputs at the anchor point values:

$$\mathbf{X} = \mathbf{X}_0|_U \quad (5)$$

$$\mathbf{U} = \mathbf{U}_0|_U \quad (6)$$

$$\mathbf{Y} = \mathbf{Y}_0|_U \quad (7)$$

which is crucial for good fidelity in piloted simulation.

As  $u$  is included as a state, a subtle yet important detail becomes evident from Eq. (3) that all stability derivatives for forward speed perturbation  $u$  (i.e.,  $X_u$ ,  $Z_u$ ,  $M_u$ , etc.) are nulled-out (multiplied by 0) because the instantaneous  $x$ -body axis airspeed  $U$  (the query for the table lookup) and the returned table value of  $x$ -body axis airspeed are always identical (i.e.,  $U|_U = U$  and therefore  $U - U|_U = 0$ ). As a result, the  $u$ -speed derivatives can be omitted from the model. However, the effect of these nulled-out derivatives is preserved and is contained implicitly in the speed variation of the trim states and controls, so the dynamic response of the anchor point model is maintained.

To demonstrate the implicit preservation of the  $u$ -speed derivatives, consider the three-DOF longitudinal equation of motion for the  $x$ -body axis:

$$\dot{U} = -QW + \bar{X} \quad (8)$$

where  $\bar{X}$ , the total specific  $x$ -force, is defined as the total  $x$ -force divided by the aircraft mass, and is the sum of the specific gravity  $x$ -force and the specific aerodynamic  $x$ -force:

$$\bar{X} \equiv X/m = \bar{X}_{\text{grav}} + \bar{X}_{\text{aero}} \quad (9)$$

The specific gravity and aerodynamic  $x$ -forces can be written as Taylor series expansions for small perturbation motion about the reference trim airspeed  $U_0$ . The specific gravity  $x$ -force expands to

$$\bar{X}_{\text{grav}} = \bar{X}_{\text{grav}_0} - (g \cos \Theta_0) (\Theta - \Theta_0) \quad (10)$$

where  $\bar{X}_{\text{grav}_0} = -g \sin \Theta_0$ . The specific aerodynamic  $x$ -force expands to

$$\begin{aligned} \bar{X}_{\text{aero}} = & \bar{X}_{\text{aero}_0} + X_u|_{U_0} (U - U_0) + X_w|_{U_0} (W - W_0) + X_q|_{U_0} (Q - Q_0) \\ & + X_{\delta_e}|_{U_0} (\delta_e - \delta_{e_0}) + X_{\delta_t}|_{U_0} (\delta_t - \delta_{t_0}) \end{aligned} \quad (11)$$

in which  $\delta_e$  is elevator deflection and  $\delta_t$  is engine thrust.

At the rectilinear trim condition, the trim aerodynamic  $x$ -force balances the trim gravity  $x$ -force:

$$\bar{X}_{\text{aero}_0} = -\bar{X}_{\text{grav}_0} = g \sin \Theta_0 \quad (12)$$

and Eq. (11) becomes

$$\begin{aligned} \bar{X}_{\text{aero}} = & g \sin \Theta_0 + X_u|_{U_0} (U - U_0) + X_w|_{U_0} (W - W_0) + X_q|_{U_0} Q \\ & + X_{\delta_e}|_{U_0} (\delta_e - \delta_{e_0}) + X_{\delta_t}|_{U_0} (\delta_t - \delta_{t_0}) \end{aligned} \quad (13)$$

Continuous full flight-envelope simulation is achieved as in Eqs. (3) and (4) by rewriting the Taylor series expansion of Eq. (13) about the instantaneous  $x$ -body airspeed  $U$ :

$$\begin{aligned} \bar{X}_{\text{aero}} = & g \sin \Theta_0|_U + X_w|_U (W - W_0|_U) + X_q|_U Q \\ & + X_{\delta_e}|_U (\delta_e - \delta_{e_0}|_U) + X_{\delta_t}|_U (\delta_t - \delta_{t_0}|_U) \end{aligned} \quad (14)$$

noting that  $U - U_0|_U = 0$  at all times, thus the term  $X_u|_U (U - U_0|_U)$  is omitted. The stability and control derivatives and trim data are then interpolated for the instantaneous  $x$ -body axis airspeed  $U$ .

Finally, the effective, implicit representation of the speed-damping derivative  $X_u$  is found by taking the partial derivative of Eq. (14) with respect to independent perturbations in  $u$ :

$$\begin{aligned} X_u \equiv \frac{\partial \bar{X}_{\text{aero}}}{\partial u} = & g \cos \Theta_0|_U \left( \frac{\partial \Theta_0|_U}{\partial u} \right) - X_w|_U \left( \frac{\partial W_0|_U}{\partial u} \right) \\ & - X_{\delta_e}|_U \left( \frac{\partial \delta_{e_0}|_U}{\partial u} \right) - X_{\delta_t}|_U \left( \frac{\partial \delta_{t_0}|_U}{\partial u} \right) \end{aligned} \quad (15)$$

Analogous derivations are used to find the implicit representations of  $Z_u$  and  $M_u$ .

Equation (15), as introduced in Tischler,<sup>1</sup> demonstrates that although the explicit  $X_u$  term is nulled by the Taylor series expansion in Eq. (14) its effect is preserved implicitly in the variation of the trim states and controls with  $x$ -body airspeed  $U$ . This concept of implicit speed derivatives is fundamental to the model stitching technique, and will be referenced throughout this paper.

Figure 1 shows an example comparison of the values of the implicit expressions for  $X_u$ ,  $Z_u$ , and  $M_u$  with the truth explicit derivative values from the AAA linear point models over a range of airspeeds at a constant altitude. As can be seen, the effective, implicit representations of the  $u$ -speed derivatives are very accurate, with small differences due to higher-order terms and linear gradients taken between the discrete points. This validates the model stitching equation of Eq. (15).

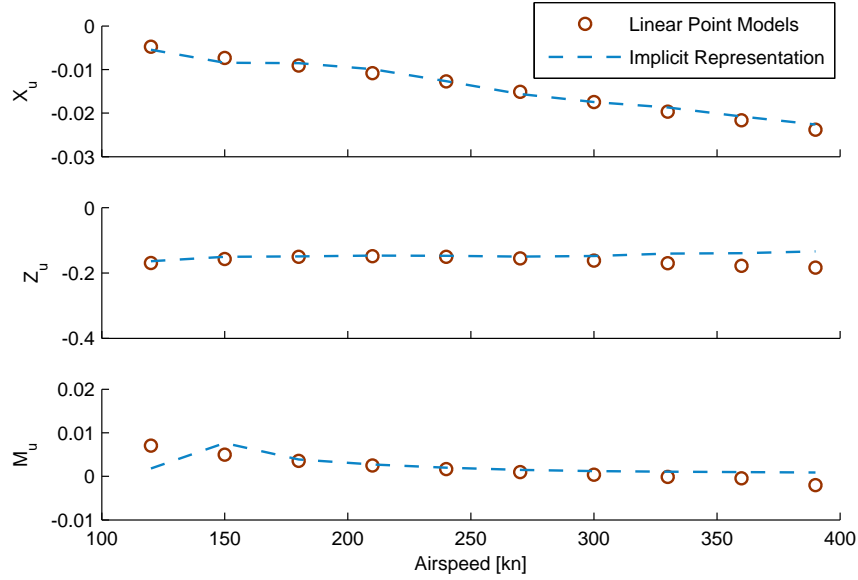


Figure 1. Implicit vs. explicit values of  $u$ -speed derivatives, CJ1 stitched model.

### C. Key Simulation Elements

Section II.B provided some basic theoretical concepts of the model stitching technique. In practice, the model stitching equations are implemented as individual elements in block-diagram form. As a collection, the model stitching elements, along with off-nominal extrapolation methods and additional features, form the *model stitching simulation architecture*.

Figure 2 shows a top-level schematic of the model stitching architecture, illustrating all of the key simulation elements. Each element will be discussed briefly, and the corresponding numbered labels in Figure 2 will be referenced. See Tobias and Tischler<sup>10</sup> for complete implementation details.

#### 1. State and Control Perturbations

Given the current  $x$ -body airspeed  $U$ , table look-ups are performed to find the vectors of trim aircraft states  $\mathbf{X}_0$  and trim controls  $\mathbf{U}_0$ . With the current aircraft state vector  $\mathbf{X}$  and current control vector  $\mathbf{U}$ , the state perturbation vector  $\Delta\mathbf{x}$  and control perturbation vector  $\Delta\mathbf{u}$  are determined:

$$\Delta\mathbf{x} \equiv \mathbf{X} - \mathbf{X}_0|_U \quad (16)$$

$$\Delta\mathbf{u} \equiv \mathbf{U} - \mathbf{U}_0|_U \quad (17)$$

This arithmetic is shown schematically in Figure 2 at labels ① and ②. The state and control perturbation vectors are used in the calculation of aerodynamic perturbation forces and moments (see Section 2).

#### 2. Aerodynamic Perturbation Forces and Moments

Aerodynamic perturbation forces and moments are calculated based on the state and control perturbation vectors found in Equations (16) and (17). This process involves performing table look-ups of the dimensional stability and control derivatives at the current airspeed. For use in the model stitching architecture, we introduce the aerodynamic  $\mathbf{A}_{\text{aero}}$  and  $\mathbf{B}_{\text{aero}}$  matrices that contain the dimensional stability and control derivatives only; they do not contain gravity or Coriolis terms. These matrices also do not include Euler angle states  $[\phi \ \theta \ \psi]$  as kinematics are included in the nonlinear equations of motion, as discussed in Section 7.

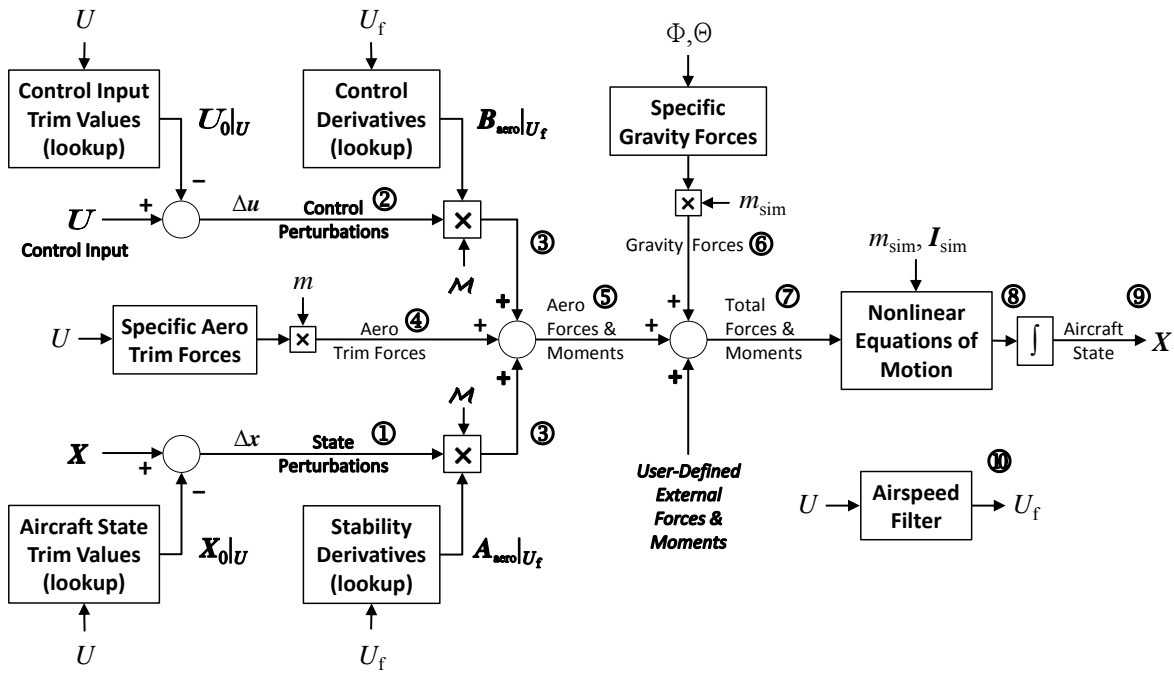


Figure 2. Model stitching architecture – top level schematic.

TECHNOLOGY DRIVEN. WARFIGHTER FOCUSED.

1

These aerodynamic matrices are given as

$$A_{\text{aero}} = \begin{bmatrix} X_u & X_v & X_w & X_p & X_q & X_r \\ Y_u & Y_v & Y_w & Y_p & Y_q & Y_r \\ Z_u & Z_v & Z_w & Z_p & Z_q & Z_r \\ L'_u & L'_v & L'_w & L'_p & L'_q & L'_r \\ M'_u & M'_v & M'_w & M'_p & M'_q & M'_r \\ N'_u & N'_v & N'_w & N'_p & N'_q & N'_r \end{bmatrix}_{6 \times 6} \quad (18)$$

$$B_{\text{aero}} = \begin{bmatrix} X_{\delta_1} & X_{\delta_2} & \dots & X_{\delta_{n_c}} \\ Y_{\delta_1} & Y_{\delta_2} & \dots & Y_{\delta_{n_c}} \\ Z_{\delta_1} & Z_{\delta_2} & \dots & Z_{\delta_{n_c}} \\ L'_{\delta_1} & L'_{\delta_2} & \dots & L'_{\delta_{n_c}} \\ M_{\delta_1} & M_{\delta_2} & \dots & M_{\delta_{n_c}} \\ N'_{\delta_1} & N'_{\delta_2} & \dots & N'_{\delta_{n_c}} \end{bmatrix}_{6 \times n_c} \quad (19)$$

For the current demonstration, these matrices have dimensions of  $6 \times 6$  and  $6 \times 4$ . A low-pass filtered  $x$ -body airspeed  $U_f$  (see Eq. (26)) is used in the look-ups of the dimensional stability and control derivatives to ensure that the derivative values remain constant for short-term motion, thereby retaining accurate dynamic responses at the discrete anchor points.

Next, the dimensional mass matrix  $\mathcal{M}$ , which is comprised of the aircraft mass  $m$  and inertia tensor  $\mathbf{I}$ , is multiplied into the matrix of stability derivatives  $A_{\text{aero}}$  and the state perturbation vector  $\Delta \mathbf{x}$  to yield a vector of aerodynamic dimensional perturbation forces and moments. Likewise, the mass matrix is multiplied into the matrix of control derivatives  $B_{\text{aero}}$  and the control perturbation vector  $\Delta \mathbf{u}$  to produce a vector of dimensional perturbation control forces and moments. The sum of both vectors yields the complete aerodynamic dimensional perturbation forces and moments, as shown schematically in Figure 2 by labels numbered ③.

### 3. Aerodynamic Trim Forces

This element determines the dimensional aerodynamic trim forces based on the trim aircraft attitude at the current airspeed. A lookup is first performed to find the trim Euler angles at the current  $x$ -body airspeed

U. Subsequently, the *specific* aerodynamic trim forces are obtained as follows:

$$\bar{X}_{\text{aero}_0} = g \sin \Theta_0|_U \quad (20)$$

$$\bar{Y}_{\text{aero}_0} = -g \cos \Theta_0|_U \sin \Phi_0|_U \quad (21)$$

$$\bar{Z}_{\text{aero}_0} = -g \cos \Theta_0|_U \cos \Phi_0|_U \quad (22)$$

The specific aerodynamic trim forces are then multiplied by the aircraft mass  $m$  to obtain the dimensional aerodynamic trim forces, which is shown schematically in Figure 2 at label ④.

#### 4. Total Aerodynamic Forces and Moments

Calculating the total dimensional aerodynamic forces and moments combines the components covered thus far. The dimensional perturbation forces and moments are summed with the dimensional aerodynamic trim forces to yield the total aerodynamic forces and moments. This summation is shown graphically at label ⑤ in Figure 2.

#### 5. Nonlinear Gravity Forces

As previously mentioned, the model stitching architecture incorporates nonlinear gravity force equations. Given the current aircraft state, the total Euler angles are used to compute the nonlinear *specific* gravity forces acting at the CG as follows:

$$\bar{X}_{\text{grav}} = -g \sin \Theta \quad (23)$$

$$\bar{Y}_{\text{grav}} = g \cos \Theta \sin \Phi \quad (24)$$

$$\bar{Z}_{\text{grav}} = g \cos \Theta \cos \Phi \quad (25)$$

At trim, note that the specific aerodynamic trim forces [Eqs. (20–22)] must balance these specific gravity forces. The specific gravity forces are then multiplied by the current *simulation value* of aircraft mass  $m_{\text{sim}}$  to obtain the dimensional gravity forces. The dimensional gravity force calculation is shown diagrammatically at label ⑥ in Figure 2.

The current simulation value of aircraft mass, which is not necessarily the mass value associated with the baseline/identified anchor point models, is utilized here to simulate off-nominal aircraft weight; see Section E for a discussion on off-nominal weight extrapolation.

#### 6. Total Forces and Moments

The aerodynamic forces and moments are summed with the nonlinear gravity forces to yield the total external, dimensional forces and moments acting at the CG. This summation is shown schematically at label ⑦ in Figure 2. The total forces and moments may be augmented with user-specified external forces and moments for the simulation of additional modeling components (e.g., landing gear).

#### 7. Nonlinear Equations of Motion

Another nonlinear component incorporated in the model stitching simulation architecture, aside from the previously discussed nonlinear gravity forces, is Newton’s nonlinear equations of motion. The inputs to the equations of motion are the total forces and moments about the aircraft CG, the current aircraft state, and simulation values of mass and inertia. The 6-DOF body-axes nonlinear equations of motion are implemented to obtain the fuselage linear and angular accelerations (refer to label ⑧ in Figure 2).

Total values of body-axes accelerations  $[\ddot{U} \ \ddot{V} \ \ddot{W}]$ , body-axes angular accelerations  $[\ddot{P} \ \ddot{Q} \ \ddot{R}]$ , and Euler-angle rates  $[\dot{\Phi} \ \dot{\Theta} \ \dot{\Psi}]$  are collated to form the 6-DOF total state-dot vector. The 6-DOF state-dot vector is then integrated to obtain the updated 6-DOF aircraft state vector, as depicted at label ⑨ in Figure 2.

#### 8. Airspeed Filter

The final key element of the model stitching simulation architecture is the airspeed filter. A low-pass filtered airspeed is used for look-up of the stability and control derivatives only (Section 2):

$$U_f = \frac{\omega_f}{s + \omega_f} U \quad (26)$$

Applying the filter ensures that the derivative values remain constant for short-term motion, thereby retaining accurate dynamic responses at the discrete anchor points. The airspeed filter and output filtered  $x$ -body airspeed  $U_f$  are shown schematically at label ⑩ in Figure 2. A break frequency of  $\omega_f = 0.2$  rad/sec has been found to be satisfactory, in that it corresponds to the lower end of the frequency range of applicability for most identified models and yet is still fast enough to allow accurate simulation of moderately-aggressive acceleration/deceleration.<sup>1</sup>

#### D. Additional Elements

Aside from the core simulation elements discussed in Section C, there are a number of additional modeling elements incorporated into the model stitching architecture. These elements include a standard atmosphere model, modeling of atmospheric disturbances (steady wind and turbulence), and a provision for user-defined external forces and moments (for the modeling of landing gear, component drag, etc.). See Section III.D for the business jet specific features included in the CJ1 stitched model.

#### E. Extrapolation to Off-Nominal Loading Configurations and Altitude

Simulation of off-nominal loading configurations, i.e., configurations with values of aircraft mass, inertia, and/or CG location that differ from the identified/baseline values, is easily accomplished using the model stitching architecture. This capability can be used to simulate an alternate trim weight, as well as continuous, real-time simulation of fuel burn-off and changes in inertia/CG location due to external stores, for example. Though mass, inertia, and CG are physically related, these parameters can be adjusted independently within the model stitching architecture. Details of the extrapolation methods are available in a forthcoming Technical Memorandum.<sup>10</sup>

Off-nominal weight and inertia are simulated by replacing the identified/baseline values of mass used to scale the nonlinear specific gravity forces (Section II.C.5) and the values of mass and inertia tensor used in the nonlinear equations of motion (Section II.C.7) with those of the current simulation configuration. The simulation mass and inertia tensor, denoted by  $m_{sim}$  and  $I_{sim}$ , are incorporated as shown in Figure 2.

An alternate CG location may be simulated given an offset vector, which defines the desired simulation CG location with respect to the original/identified CG location. First, the simulation body-axes velocity components and angular rates are transformed to find the body-axes velocity components at the original CG location. These transformed velocity components are then used in the look-ups to obtain the trim states, trim controls, and corresponding perturbation vectors. Finally, the computed forces and moments are transformed to the simulated CG location, providing an accurate dynamic response.

For simulation of alternate altitudes, the dimensional stability and control derivatives (Section II.C.2) and specific aerodynamic trim forces (Section II.C.3) are scaled by the air density ratio  $\rho_{sim}/\rho$ , which is the ratio of air density at the simulation altitude to that at the altitude at which the models were identified or configured. Then, the stitched model is retrimmed to account for the changes in lift and drag at the off-nominal altitude condition. This method ignores any nonlinear effects, such as engine performance with variations in air density or variation of the nondimensional derivatives as a function of angle of attack.

### III. Stitched Simulation Model of Cessna CJ1

A stitched simulation model of a light business jet, representative of the Cessna Citation CJ1 (Model 525), was developed using the model stitching simulation architecture, as discussed in Section II.C, and discrete point linear models derived from DARcorporation’s Advanced Aircraft Analysis<sup>2</sup> (AAA) software. AAA was configured using the Cessna 525 model included with the software to generate nondimensional stability and control derivatives, along with corresponding trim data, for a collection of discrete flight conditions. Post-processing was performed on the AAA data to convert the output nondimensional derivatives into dimensional, body-axes derivatives for the formulation of state-space point models. Additional modeling features, including flap effects and a simple engine model, were integrated into the CJ1 stitched model for added fidelity in full-mission piloted simulation. Results are presented verifying the extrapolation methods used in the model stitching architecture for off-nominal loading configurations and flight conditions.

## A. Bare-Airframe Model Description

AAA was configured for a light business jet representative of the Cessna Citation CJ1 (Model 525), shown in Figure 3. The model is a twin turbopfan-powered light business jet capable of carrying up to seven passengers. It has a wingspan of 46 ft 11 in, a length of 42 ft 7 in, a typical empty weight of 6,765 lb, and a maximum takeoff weight (MTOW) of 10,700 lb. The model has a maximum cruise speed of 389 KTAS, a range of about 1,300 nm, and a service ceiling of 41,000 ft.



Figure 3. Typical light business jet – Cessna Citation CJ1 (Model 525).

## B. State-Space Point Models

### 1. AAA Software

Advanced Aircraft Analysis<sup>2</sup> (AAA) is an aircraft design and stability/control analysis software tool produced by DARcorporation. AAA employs design methodology from classical textbooks, digital DATCOM, and wind tunnel test data to calculate the aerodynamics of the configured aircraft model at user-specified flight conditions. AAA was configured using the Cessna 525 model included with the software to obtain the results presented herein.

### 2. State-Space Formulation

The model stitching simulation architecture discussed in Section II is designed to accommodate both fixed-wing aircraft and rotorcraft, and requires the state-space models to be formulated using dimensional stability and control derivatives in *body axes*. AAA generates nondimensional derivatives in stability axes, so transformations were necessary. Using methods and equations covered in Stevens and Lewis<sup>11</sup> and McRuer et al.,<sup>12</sup> the nondimensional, stability-axes stability and control derivatives from AAA are transformed into dimensional, body-axes stability and control derivatives. A simple schematic is provided in Figure 4 which shows the transformation from AAA output to formulated state-space matrices.

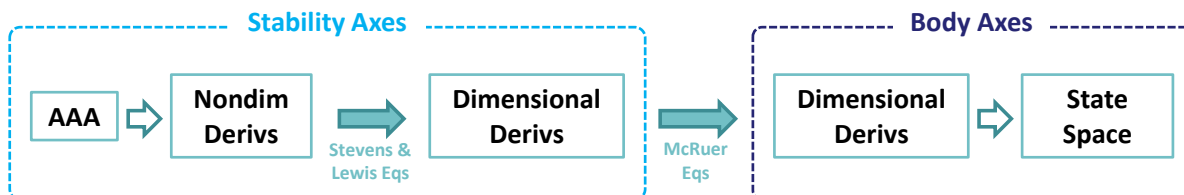


Figure 4. Transformation of stability and control derivatives.

The complete 6-DOF state space formulation for the AAA CJ1 point models is given in body axes as:<sup>12</sup>

$$\begin{bmatrix} 1 & 0 & -X_{\dot{w}} & 0 & 0 & 0 & 0 & 0 \\ 0 & 1 & 0 & 0 & 0 & 0 & 0 & 0 \\ 0 & 0 & 1 - Z_{\dot{w}} & 0 & 0 & 0 & 0 & 0 \\ 0 & 0 & 0 & 1 & 0 & 0 & 0 & 0 \\ 0 & 0 & -M_{\dot{w}} & 0 & 1 & 0 & 0 & 0 \\ 0 & 0 & 0 & 0 & 0 & 1 & 0 & 0 \\ 0 & 0 & 0 & 0 & 0 & 0 & 1 & 0 \\ 0 & 0 & 0 & 0 & 0 & 0 & 0 & 1 \end{bmatrix} \begin{bmatrix} \dot{u} \\ \dot{v} \\ \dot{w} \\ \dot{p} \\ \dot{q} \\ \dot{r} \\ \dot{\phi} \\ \dot{\theta} \end{bmatrix} = \begin{bmatrix} X_u & 0 & X_w & 0 & X_q - W_0 & V_0 & 0 & -g \cos \Theta_0 \\ 0 & Y_v & 0 & Y_p + W_0 & 0 & Y_r - U_0 & g \cos \Theta_0 & 0 \\ Z_u & 0 & Z_w & -V_0 & Z_q + U_0 & 0 & 0 & -g \sin \Theta_0 \\ 0 & L'_v & 0 & L'_p & 0 & L'_r & 0 & 0 \\ M_u & 0 & M_w & 0 & M_q & 0 & 0 & 0 \\ 0 & N'_v & 0 & N'_p & 0 & N'_r & 0 & 0 \\ 0 & 0 & 0 & 1 & 0 & \tan \Theta_0 & 0 & 0 \\ 0 & 0 & 0 & 0 & 1 & 0 & 0 & 0 \end{bmatrix} \begin{bmatrix} u \\ v \\ w \\ p \\ q \\ r \\ \phi \\ \theta \end{bmatrix} \quad (27)$$

$$+ \begin{bmatrix} 0 & X_{\delta_e} & 0 & X_{\delta_t} \\ Y_{\delta_a} & 0 & Y_{\delta_r} & 0 \\ 0 & Z_{\delta_e} & 0 & Z_{\delta_t} \\ L'_{\delta_a} & 0 & L'_{\delta_r} & 0 \\ 0 & M_{\delta_e} & 0 & M_{\delta_t} \\ N'_{\delta_a} & 0 & N'_{\delta_r} & 0 \\ 0 & 0 & 0 & 0 \\ 0 & 0 & 0 & 0 \end{bmatrix} \begin{bmatrix} \delta_a \\ \delta_e \\ \delta_r \\ \delta_t \end{bmatrix}$$

$\mathbf{A}_{\text{aero}}$  and  $\mathbf{B}_{\text{aero}}$  matrices are employed in the model stitching architecture, as discussed in Section II.C.2, which contain only the dimensional aerodynamic stability and control derivatives. Equation (27) is first rewritten in conventional  $\dot{\mathbf{x}} = \mathbf{A}\mathbf{x} + \mathbf{B}\mathbf{u}$  form, and the gravity terms (e.g.,  $g \cos \Theta_0$ ), Coriolis terms (e.g.,  $-W_0$ ), and Euler angle states ( $\phi$  and  $\theta$ ) are removed giving

$$\mathbf{A}_{\text{aero}} = \begin{bmatrix} X_u + \frac{Z_u X_{\dot{w}}}{1 - Z_{\dot{w}}} & 0 & X_w + \frac{Z_w X_{\dot{w}}}{1 - Z_{\dot{w}}} & 0 & X_q + \frac{Z_q X_{\dot{w}}}{1 - Z_{\dot{w}}} & 0 \\ 0 & Y_v & 0 & Y_p & 0 & Y_r \\ \frac{Z_u}{1 - Z_{\dot{w}}} & 0 & \frac{Z_w}{1 - Z_{\dot{w}}} & 0 & \frac{Z_q}{1 - Z_{\dot{w}}} & 0 \\ 0 & L'_v & 0 & L'_p & 0 & L'_r \\ M_u + \frac{Z_u M_{\dot{w}}}{1 - Z_{\dot{w}}} & 0 & M_w + \frac{Z_w M_{\dot{w}}}{1 - Z_{\dot{w}}} & 0 & M_q + \frac{Z_q M_{\dot{w}}}{1 - Z_{\dot{w}}} & 0 \\ 0 & N'_v & 0 & N'_p & 0 & N'_r \end{bmatrix}_{6 \times 6} \quad (28)$$

$$\mathbf{B}_{\text{aero}} = \begin{bmatrix} 0 & X_{\delta_e} + \frac{Z_{\delta_e} X_{\dot{w}}}{1 - Z_{\dot{w}}} & 0 & X_{\delta_t} + \frac{Z_{\delta_t} X_{\dot{w}}}{1 - Z_{\dot{w}}} \\ Y_{\delta_a} & 0 & Y_{\delta_r} & 0 \\ 0 & \frac{Z_{\delta_e}}{1 - Z_{\dot{w}}} & 0 & \frac{Z_{\delta_t}}{1 - Z_{\dot{w}}} \\ L'_{\delta_a} & 0 & L'_{\delta_r} & 0 \\ 0 & M_{\delta_e} + \frac{Z_{\delta_e} M_{\dot{w}}}{1 - Z_{\dot{w}}} & 0 & M_{\delta_t} + \frac{Z_{\delta_t} M_{\dot{w}}}{1 - Z_{\dot{w}}} \\ N'_{\delta_a} & 0 & N'_{\delta_r} & 0 \end{bmatrix}_{6 \times 4} \quad (29)$$

### 3. Model Limitations

The AAA CJ1 models are accurate over most of the relevant flight envelope, but do not include certain nonlinearities, such as stall, departure, and aerobatic dynamics. These edge-of-the-envelope conditions are considered for this application to be outside the flight envelope of interest for this study. Additionally, the models do not include structural flexibility effects.

## C. Flight Conditions

As mentioned in the discussion of model stitching basic concepts in Section II.B, the key requirement for a full flight-envelope stitched simulation model is a collection of state-space models and trim data of the states and controls for several discrete flight conditions, or “anchor” points, covering a range of airspeed and perhaps altitude. The required quantity and spacing of anchor trim points and anchor point models for a high-fidelity stitched model is largely dictated by vehicle type, applicable flight envelope, and intended simulation purpose. For piloted simulation of a light business jet class of aircraft, as presented herein, which has a broad airspeed/altitude flight envelope, the dynamics must be accurately represented throughout. Of course one could generate a large collection of models to finely cover the entire flight envelope, but this approach is not only impractical for the collection of flight-identified models, in which frequency sweeps must be performed at each flight condition, but is unnecessary considering data preprocessing techniques and the inclusion of extrapolation methods within the model stitching architecture.

Preprocessing techniques include fitting data with splines to interpolate/extrapolate data with airspeed to allow fewer anchor trim points and point models, and ultimately to construct a full rectangular grid of data points with uniformly-spaced values of  $x$ -body airspeed  $U$  (for “stitching” in  $U$ ), per requirements of the model stitching architecture. Air-density scaling may then be employed in the model stitching architecture to extrapolate data from a particular altitude to a broader range of altitudes. Additionally, incorporated into the model stitching simulation architecture are extrapolation methods for the simulation of off-nominal aircraft loading configurations, including variations in weight, inertia, and center of gravity, without the need for additional data. This allows models of a single baseline (nominal) configuration to be used to simulate a wide range of flight conditions and loading configurations throughout.

The CJ1 stitched simulation model presented herein was developed using the above preprocessing techniques, keeping flight-test implications in mind. A demonstration of the complete process is presented below, with example data in Figure 5 referenced throughout.

A series of AAA models was first generated covering a range of true airspeed at two altitudes: 10,000 ft and 30,000 ft. The method described in Section III.B.2 was then employed to produce four body-axis dimensional state-space anchor point models at each altitude, indicated by the solid circle markers shown in Figure 5(a). Additionally, trim data alone were taken from the remaining AAA models to incorporate finely-spaced anchor trim points, as indicated by the empty square markers in (a). Note that trim data are included with each anchor point model, as well. A depiction of a representative flight envelope is included with the anchor points to show the broad spacing of anchor point models and more finely-spaced anchor trim points covering the airspeed envelope. Values of the corresponding trim thrust,  $\delta_t$ , and directional static-stability derivative  $N_v$  are shown in (d) and (g), respectively.

Next, the trim data and stability and control derivatives from the anchor points are fit with cubic splines and interpolated to fine, evenly-spaced values of airspeed  $U$  in 10-ft/sec increments. The resulting full rectangular grid defined by airspeed  $U = [130:10:700]$  and altitude  $= [10000 \ 30000]$  is shown in Figure 5(b). Note that some points lie outside the operational flight envelope, but it is a requirement of the model stitching architecture to have the full grid defined. As such, there are data defined for all points in the grid, even if those points would ordinarily not be flown. The spline-fit, interpolated data for thrust and  $N_v$  are shown in (e) and (h), respectively.

Finally, using the grid of data defined in Figure 5(b), which consists of the full range of airspeed at two altitudes, the air density scaling methods described in Section II.E are employed to extrapolate the data to other altitudes, and the stitched model is retrimmed. Following the guidance of the flight test implications of Section VII.D, the identified 10,000-ft data are extrapolated to sea level and 20,000 ft, and the identified 30,000-ft data are extrapolated to 40,000 ft. The retrimmed values of thrust and  $N_v$  are shown in (f) and (i), respectively. The model stitching architecture was then configured with the full rectangular grid of data and stored in table lookups to represent the bare-airframe dynamics of the CJ1 stitched simulation model.

## D. Additional Airframe-Specific Features

Additional features specific to a light business jet class of aircraft were incorporated into the CJ1 stitched model. Flap effects, simple engine models with the capability to control thrust output from each engine separately, an elementary landing gear model, and spoilers are discussed.

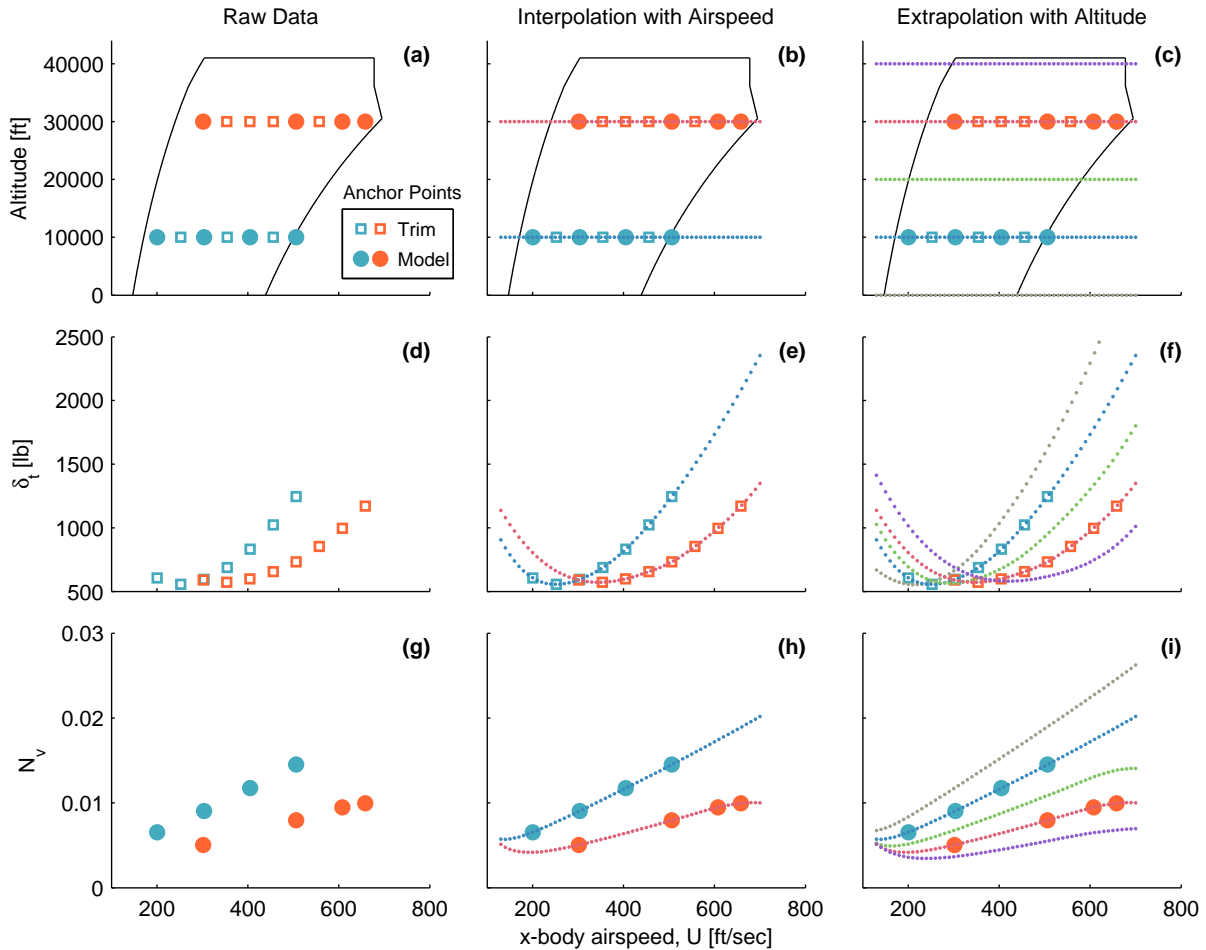


Figure 5. Spline-fit data and extrapolation to cover entire flight envelope.

### 1. Flap Effects

The aerodynamic effects of flaps on trim and bare-airframe dynamics have been integrated into the CJ1 stitched model. Scaling and corrections of the values of trim attitude, trim controls, and some secondary stability and control derivatives as a function of flap deflection and airspeed were analyzed from AAA truth models configured with two different flap settings. These correction effects were then applied to the baseline point models and stored as an additional interpolation dimension in the lookup tables of derivatives and trim. This additional interpolation dimension allows for continuous simulation of various flap settings throughout the flight envelope for piloted evaluations.

For a given flight condition, flap deflection considerably affects trim pitch attitude, elevator deflection, and thrust, but has only a minor effect on the stability and control derivatives.<sup>1</sup> Verification of flap effects in the CJ1 stitched model for deflections of 15 and 35 degrees over a range of airspeeds is provided in Section III.E.4.

### 2. Simple Engine Model

A simple engine model has been incorporated into the CJ1 stitched model, which takes input in throttle position and converts it to engine thrust in pounds. Throttle position (with a range of 0–1) is first scaled by the maximum available engine thrust to convert to commanded thrust. Maximum and idle thrust values are looked-up as functions of altitude and Mach. Finally, the engine response dynamics are modeled by a second-order transfer function with a natural frequency of 3 rad/sec and a damping ratio of 1.

Included in the engine model is the ability to control the thrust output of each of the two engines

separately. Rather than formulating the state-space models with two thrust control derivative (one for each engine), a simple moment arm component is introduced in conjunction with total thrust output. For the purposes of the current study, this feature allows the pilot to realistically employ each throttle. Asymmetric thrust could be utilized to simulate a one-engine-out condition, for example.

### 3. Simple Landing Gear

An elementary landing gear model was incorporated into the stitched simulation model, which utilizes a spring force proportional to strut displacement and body rate damping to arrest vertical motion and zero-out attitude at some height offset above ground level. Saturation logic is included to reasonably mimic separate main- and nose-gear contact; this also allows for basic rotation for takeoff. The characteristics of the landing gear were not evaluated in the fidelity assessment; however, this basic capability enables reasonable assessment of landing and touch-and-go traffic pattern flying.

### 4. Component Drag

Unlike the drag effects due to flaps which are implicitly included by scheduling trim attitude and controls with flap deflection, the drag effects due to the deployment of landing gear and spoilers are incorporated in the stitched model through an external force. Each drag component is modeled as an equivalent flat-plate drag area and scaled by dynamic pressure and deployment amount to obtain dimensional drag force in pounds. Total drag of all components is summed and input as an external force vector into the nonlinear equations of motion (see external force vector shown schematically in Figure 2).

## E. Verification of Extrapolation Methods

The model stitching architecture incorporates extrapolation methods which allow simulation of off-nominal aircraft loading configurations, as discussed in Section II.E. In order to verify the extrapolation methods used to simulate off-nominal loading configurations in the CJ1 stitched model, a collection of AAA truth models were generated covering ranges of airspeed, gross weight, and fuselage-station CG locations. Additionally, altitude extrapolation via density scaling is employed and the results are compared to a collection of AAA truth models covering the full-flight envelope altitude range.

A baseline (nominal) configuration of 8500 lb, mid CG at an altitude of 10,000 ft was chosen for the AAA anchor point models and anchor trim points used in the stitched model for all results presented in this section. The stitched model, configured with only these baseline anchor points, was then retrimmed and linearized at each off-nominal verification point, with the results verified against the database of AAA truth models. The results verify the built-in accommodation in the model stitching architecture for off-nominal weight, CG, and altitude (Section II.E), and the inclusion of flap effects (Section III.D.1).

### 1. Weight

Figure 6 shows results of simulating off-nominal values of weight in the CJ1 stitched model. The stitched model, configured only with anchor point models and trim data of the nominal 8500-lb configuration (solid symbols), was retrimmed and linearized for various simulation values of gross weight over a range of airspeed (dashed lines) and compared with values from the AAA truth models (solid lines). Overall, there is excellent agreement between the stitched model and the truth data.

An increase in trim angle of attack is needed with an increase in gross weight, as expected, due to greater lift required to balance the weight. This effect is seen more strongly in the lower-air-speed regime, where a greater change in angle of attack is required to generate the required lift due to lower dynamic pressure. The stitched model tracks the changes in angle of attack perfectly, as compared to the truth data. Similarly, the required trim thrust in pounds,  $\delta_t$ , increases with an increase in gross weight, but effectively only in the low- to mid-speed regime, where thrust has a greater vertical component due to the higher angles of attack. The stitched model accurately extrapolates the trim thrust required for the range of weights, with a small disparity in the simulated 6000-lb configuration at the low-speed end of the flight envelope. Pertinent stability derivatives  $Z_q$  and  $Y_v$  (analogous to  $Y_\beta$ ) agree perfectly with values from the AAA truth data. This verifies the capability to extrapolate to off-nominal values of weight using only point models of a nominal weight.

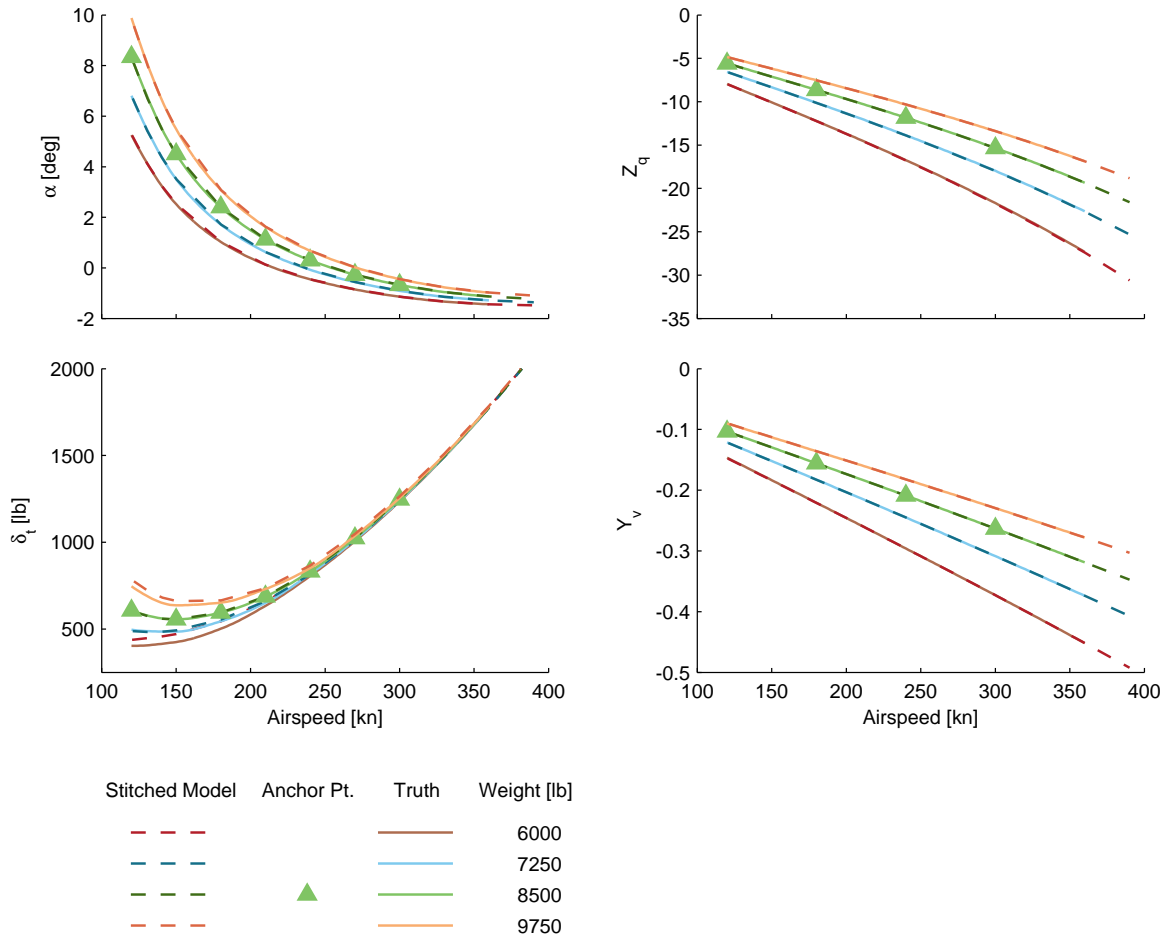


Figure 6. Off-nominal verification – weight.

## 2. Center of Gravity

Off-nominal simulation values of center of gravity (CG) location were investigated in the CJ1 stitched model. Figure 7 shows results of simulating off-nominal values of fuselage-station CG location ( $x$ -body axis, positive aft) in the CJ1 stitched model. The stitched model, configured only with anchor point models and trim data of the nominal mid-CG (244.3 in, or 22.5% MAC) configuration (solid symbols), was retrimmed and linearized for simulation values of a forward (240.1 in, or 16.5% MAC) and aft (248.4 in, or 28.5% MAC) fuselage-station CG over a range of airspeed (dashed lines) and compared with values from the AAA truth data (solid lines). Overall the stitched model agrees nearly perfectly with the truth data.

Trim elevator deflection is more downward (positive) as the CG moves aft (higher value of station CG) due to decreased download required on the tail, while trim angle of attack remains virtually unchanged (gross weight held constant). In addition, key stability derivative  $M_w$ , which is analogous to  $M_\alpha$ , decreases in magnitude, thus indicating decreased static margin, as expected for the aft CG shift. A similar trend is seen in the directional static-stability derivative  $N_v$ , which is analogous to  $N_\beta$ . This verifies the capability to extrapolate to off-nominal values of CG using only point models of a nominal CG.

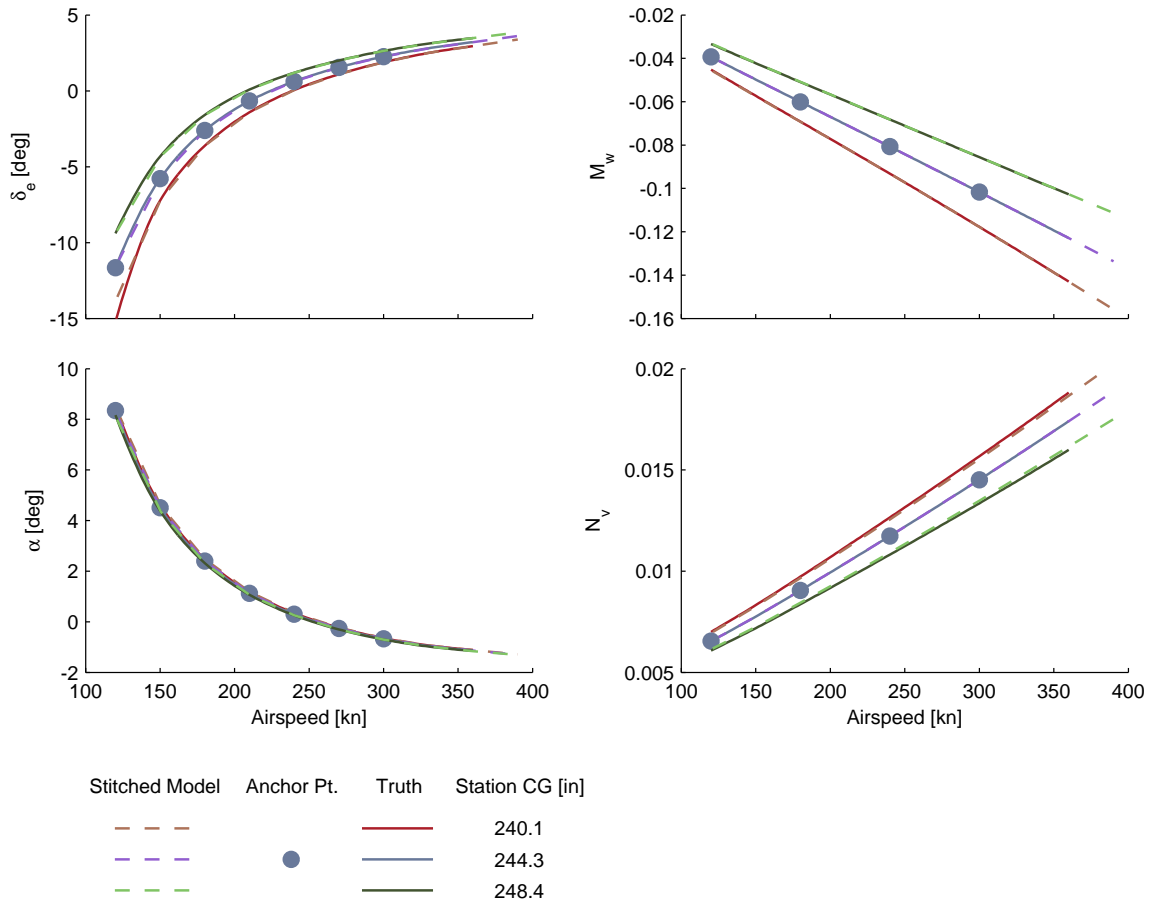


Figure 7. Off-nominal verification – fuselage-station CG.

### 3. Altitude

Simulation of alternate altitudes in the stitched model involves scaling the dimensional stability and control derivatives and specific aerodynamic trim forces by the air density ratio  $\rho_{\text{sim}}/\rho$  (the ratio of air density at the simulation altitude to that at the baseline altitude) and retrimming. The strategy implemented in this case was to perform the extrapolation based on two sets of anchor point models and trim data; one set of data configured at 10,000 ft, and the second set configured at 30,000 ft. The air-density extrapolation was then performed on each set of data and the results were combined. Specifically, the 10,000-ft data are extrapolated to sea level and 20,000 ft, and the 30,000-ft data are extrapolated to 40,000 ft, covering the entire altitude envelope in 10,000-ft increments. See the discussion of flight test implications in Section VII.D for more details on this strategy.

Figure 8 shows results of a range of simulation flight altitudes in the CJ1 stitched model. The stitched model, configured only with point models and trim data from the two anchor altitudes of 10,000 and 30,000 ft (solid symbols), was retrimmed and linearized over the full altitude/airspeed flight envelope (dashed lines) and compared with values from the AAA truth models (solid lines). Trim elevator deflection and trim thrust track nearly perfectly with the point models. The implicit  $u$ -speed derivatives are well preserved.

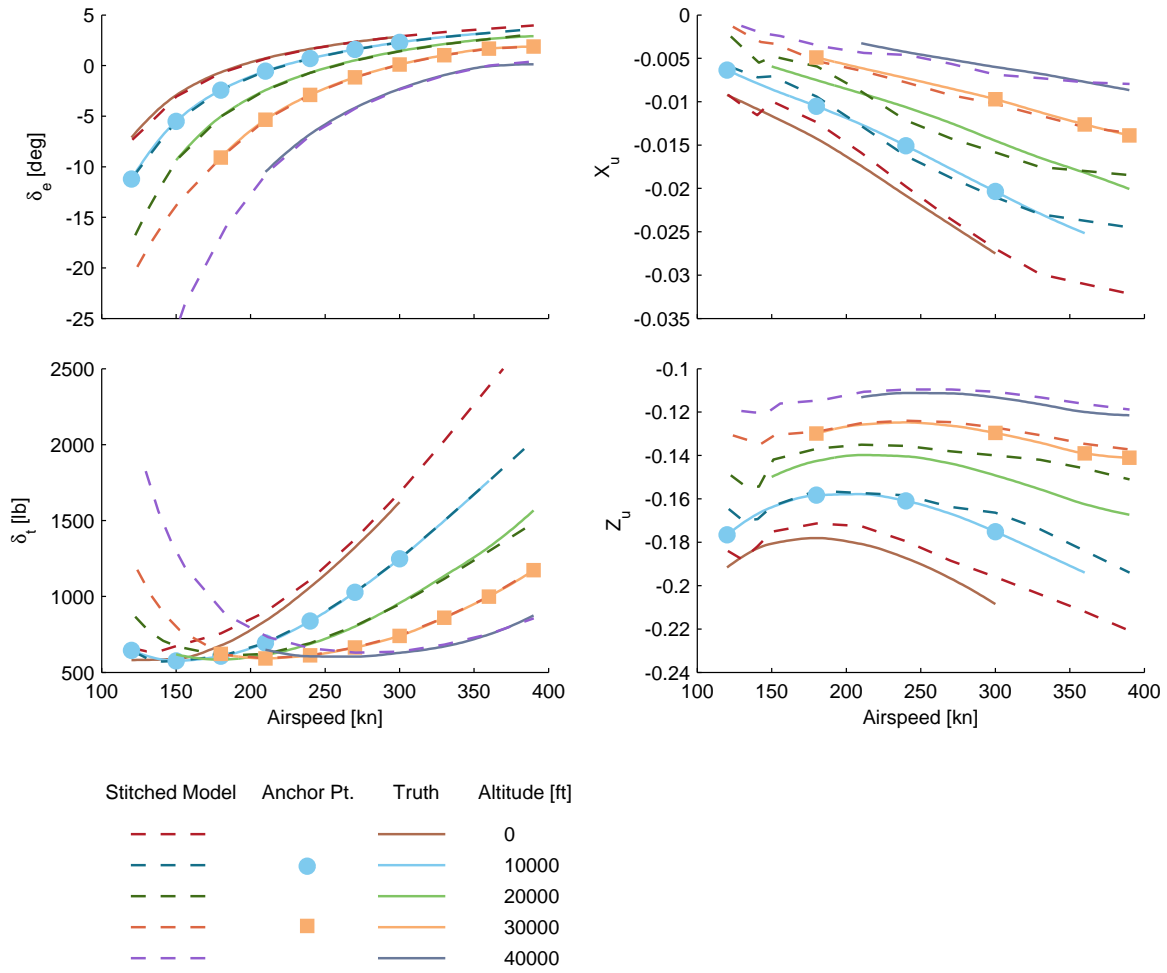


Figure 8. Verification of altitude extrapolation.

#### 4. Flap Setting

The effects of flaps are included in the CJ1 stitched model, as discussed in Section D.1. Figure 9 shows results of retrimming and linearizing the stitched model configured with two flap deflection settings compared to values from AAA truth models. For a given airspeed, an increase in flap deflection results in an increase in lift and drag, thus less angle of attack is needed and a greater total thrust is required to maintain trim. The angle of attack and thrust results from the stitched model track very well with values from the point models. The implicit  $X_u$  speed derivative agreement is very good.

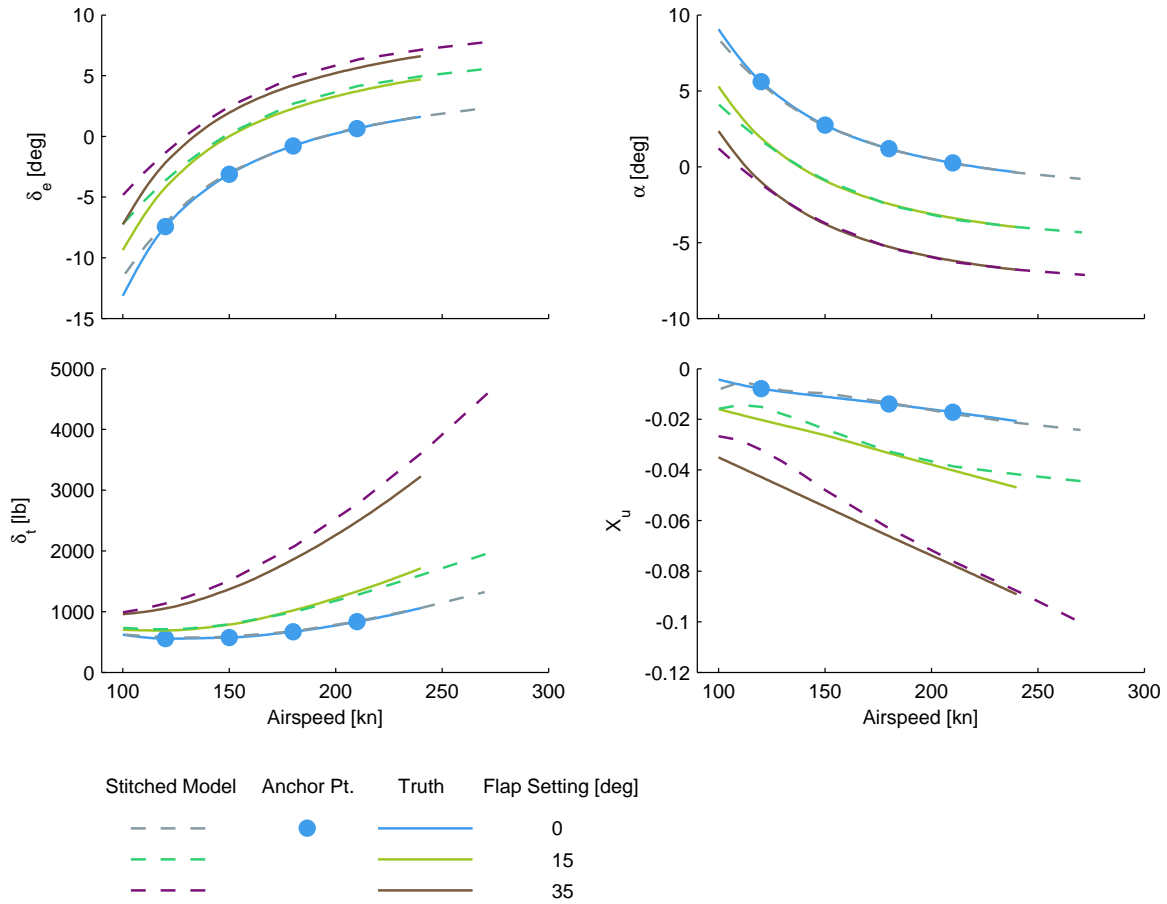


Figure 9. Off-nominal verification – flap deflection.

## IV. Simulation Facility Setup and Verification

The full flight-envelope CJ1 stitched simulation model, as presented in Section III, was evaluated within the Cessna fixed-base business jet simulator. Figure 10 shows a picture of the simulation facility, which is based on a modified Cessna Citation Excel cab. The outside visual displays provide the pilots with a 170-deg field of view, using commercially available LCD projectors. The inceptors in the cab consist of a control column and rudder pedals with control loading in both left- and right-seat positions, and conventional throttles. Communications between the stitched simulation model and the displays is accomplished via UDP packets updated at 200 Hz.

Integration of the CJ1 stitched model into Cessna’s simulator facility was verified by performing a series of dynamic response checks and piloted frequency sweeps at various flight conditions. Frequency responses of the primary on-axis responses were extracted using frequency-domain identification techniques<sup>1</sup> and compared with those of the truth point models. Total simulator processing equivalent time delay was calculated to ensure reasonable end-to-end time delay.

### A. Dynamic Response Checks

A series of dynamic response checks were performed at various flight conditions to verify integration of the CJ1 stitched simulation model into the simulator facility. This subsection presents the primary dynamic responses for Mach 0.3 (195 KTAS), 5000 ft altitude, and nominal weight and CG configuration. This flight condition is one that is at an altitude and airspeed that differs from the anchor point models, which verifies interpolation within the stitched model. A summary of the mode natural frequency and damping results for this check case is provided in Table 1. The longitudinal and lateral/directional stability and control



Figure 10. Cessna's fixed-based simulator.

derivatives are summarized in Tables 2 and 3, respectively.

Figures 11–14 show the primary longitudinal frequency responses for the check case. These responses are obtained from linearizing the stitched model to generate a Bode plot for comparison with the point model. There is near-perfect agreement between the stitched model and the point model. The short period mode is perfectly captured by the stitched model, and the phugoid mode is very closely represented (a match in natural frequency but a damping of  $\zeta = 0.049$  as compared to  $\zeta = 0.052$  for the point model, as seen in Table 1). The phugoid mode can be approximated as  $2(\zeta\omega)_P = -X_u$  from McRuer et al.,<sup>12</sup> indicating that phugoid damping is proportional to the value of  $X_u$ . With essentially equal values of phugoid natural frequency between the stitched model and the point model, this slight disparity of approximately 6% in phugoid damping can be attributed to the 6% disparity in values of  $X_u$  between the implicit representation of the stitched model compared to that of the point model, as seen in Table 2.

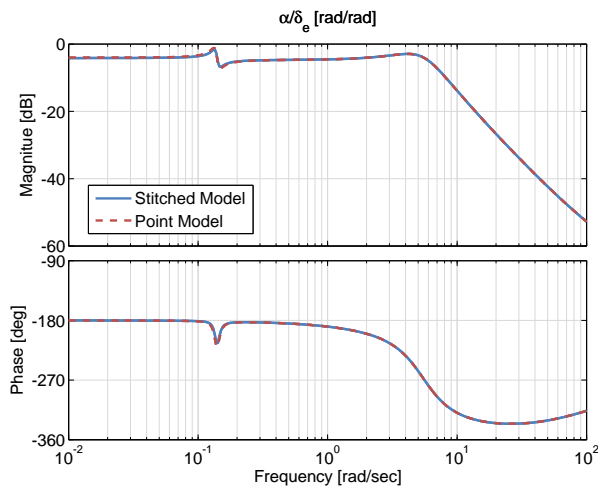


Figure 11. Check case: angle-of-attack response to elevator input comparison.

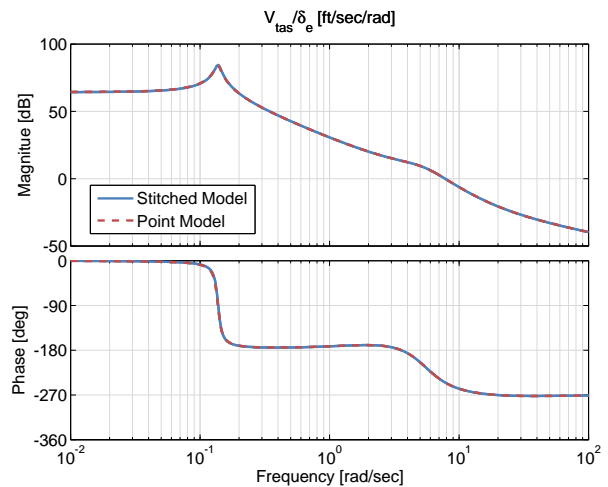


Figure 12. Check case: true airspeed response to elevator input comparison.

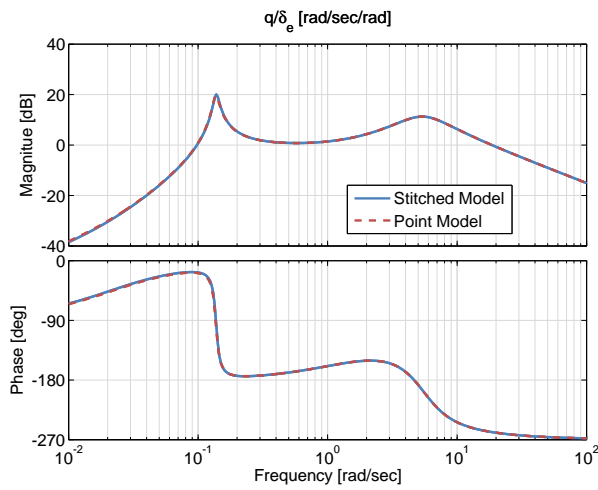


Figure 13. Check case: pitch rate response to elevator input comparison.

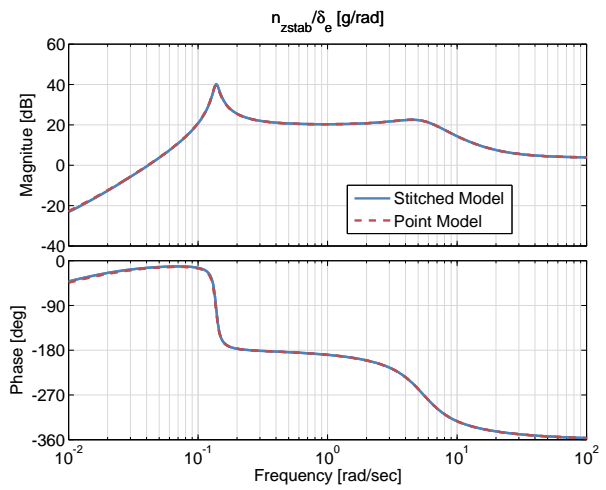


Figure 14. Check case: normal acceleration response to elevator input comparison.

Figures 15–18 show the primary lateral/directional frequency responses for the check case. There is near-perfect agreement between the stitched model and the point model for all lateral/directional modes.

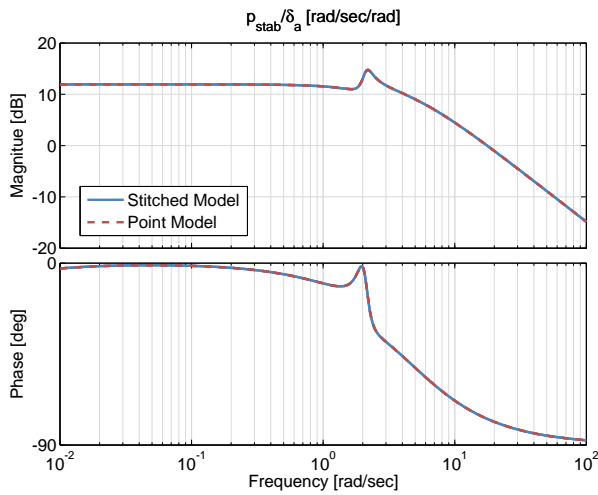


Figure 15. Check case: roll rate response to aileron input comparison.

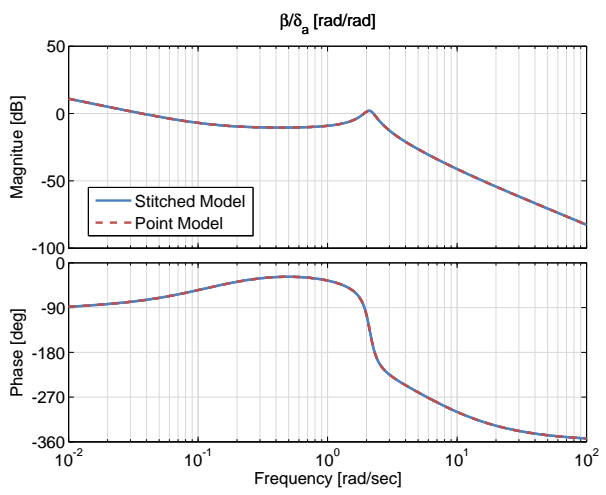


Figure 16. Check case: sideslip response to aileron input comparison.

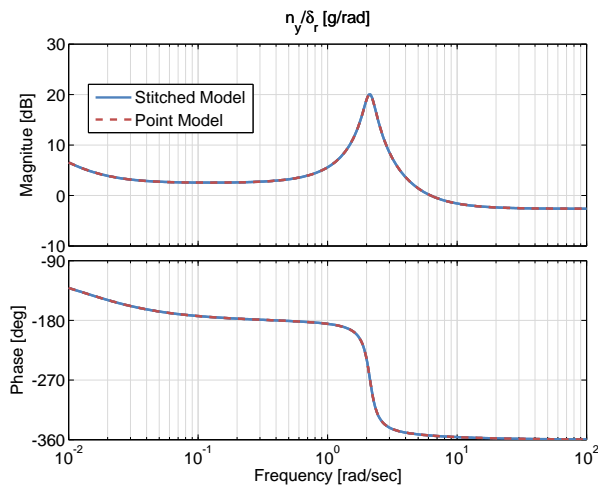


Figure 17. Check case: lateral acceleration response to rudder input comparison.

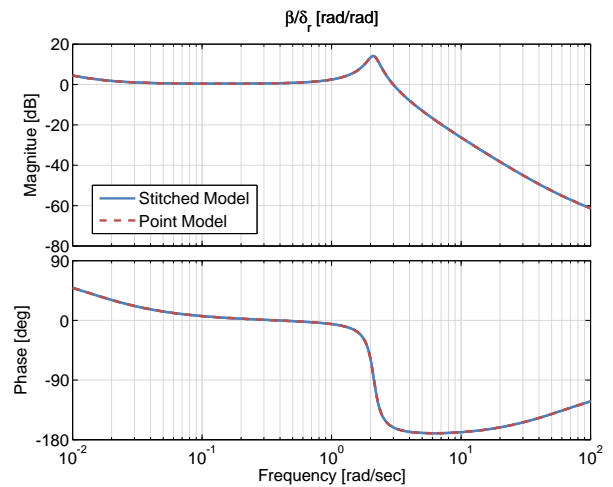


Figure 18. Check case: sideslip response to rudder input comparison.

Table 1. Check case: modes

| Mode            | Parameter            | Stitched Model | Point Model |
|-----------------|----------------------|----------------|-------------|
| Phugoid         | $\omega_n$ [rad/sec] | 0.1379         | 0.1371      |
|                 | $\zeta$              | 0.0487         | 0.0515      |
| Short Period    | $\omega_n$ [rad/sec] | 5.4745         | 5.4745      |
|                 | $\zeta$              | 0.4597         | 0.4598      |
| Spiral          | $\tau$ [sec]         | -2233.2        | -2233.8     |
| Dutch Roll      | $\omega_n$ [rad/sec] | 2.1190         | 2.1189      |
|                 | $\zeta$              | 0.1019         | 0.1019      |
| Roll Subsidence | $\tau$ [sec]         | 0.2379         | 0.2379      |

Table 2. Check case: longitudinal stability and control derivatives, body axes

| Derivative     | Stitched Model | Point Model |
|----------------|----------------|-------------|
| $X_u$          | -0.0125        | -0.0132     |
| $Z_u$          | -0.1652        | -0.1663     |
| $M_u$          | 0.0028         | 0.0027      |
| $X_w$          | 0.0801         | 0.0800      |
| $Z_w$          | -1.8684        | -1.8684     |
| $M_w$          | -0.0756        | -0.0756     |
| $X_q$          | 0.2169         | 0.2166      |
| $Z_q$          | -10.968        | -10.968     |
| $M_q$          | -3.1661        | -3.1670     |
| $X_{\delta_e}$ | -0.0267        | -0.0276     |
| $Z_{\delta_e}$ | -49.387        | -49.422     |
| $M_{\delta_e}$ | -17.599        | -17.597     |
| $X_{\delta_t}$ | 0.0038         | 0.0038      |
| $Z_{\delta_t}$ | -0.0002        | -0.0002     |
| $M_{\delta_t}$ | -0.0001        | -0.0001     |

Table 3. Check case: lateral/directional stability and control derivatives, body axes

| Derivative     | Stitched Model | Point Model |
|----------------|----------------|-------------|
| $Y_v$          | -0.1971        | -0.1971     |
| $L_v$          | -0.0217        | -0.0216     |
| $N_v$          | 0.0111         | 0.0111      |
| $Y_p$          | -0.8436        | -0.8436     |
| $L_p$          | -4.0914        | -4.0913     |
| $N_p$          | -0.4193        | -0.4193     |
| $Y_r$          | 2.2137         | 2.2137      |
| $L_r$          | 0.6004         | 0.6005      |
| $N_r$          | -0.3463        | -0.3463     |
| $L_{\delta_a}$ | 18.068         | 18.067      |
| $N_{\delta_a}$ | 1.0515         | 1.0513      |
| $Y_{\delta_r}$ | 23.768         | 23.766      |
| $L_{\delta_r}$ | 1.7534         | 1.7530      |
| $N_{\delta_r}$ | -4.5688        | -4.5684     |

Figures 19–21 show the short- and long-term time history response comparisons for the check case for three separate control doublets. Figure 19 shows the airspeed and angle-of-attack response comparisons for a 5-deg elevator doublet. Angle of attack is nearly perfectly simulated by the stitched model, and excellent agreement is seen in the airspeed response. Figure 20 shows the response comparisons of roll rate and sideslip angle for a 5-deg aileron doublet, and Figure 21 shows the lateral acceleration and sideslip-angle response comparisons for a 5-deg rudder doublet, with near-perfect agreement for all lateral/directional parameters.

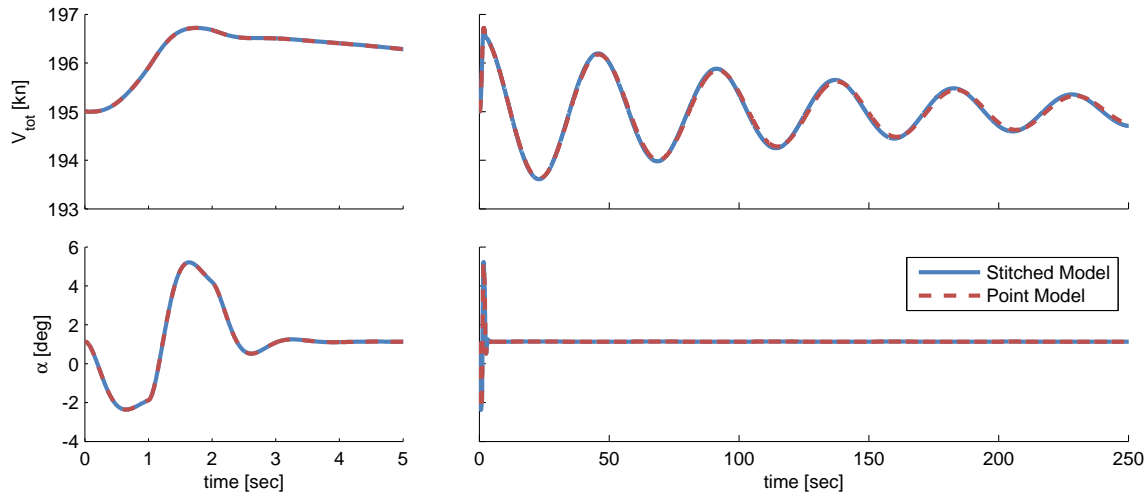


Figure 19. Check case: short- and long-term time history responses, elevator doublet.

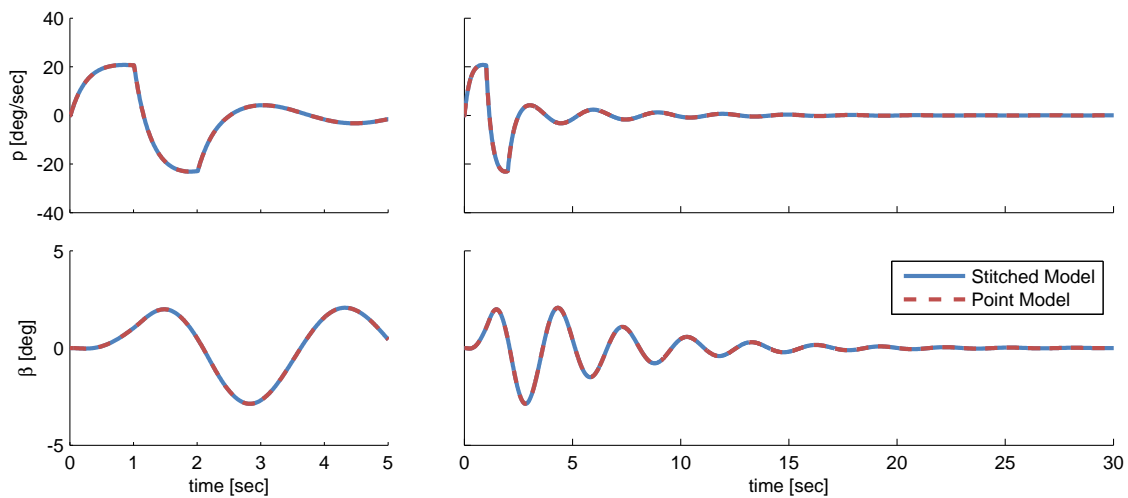


Figure 20. Check case: short- and long-term time history responses, aileron doublet.

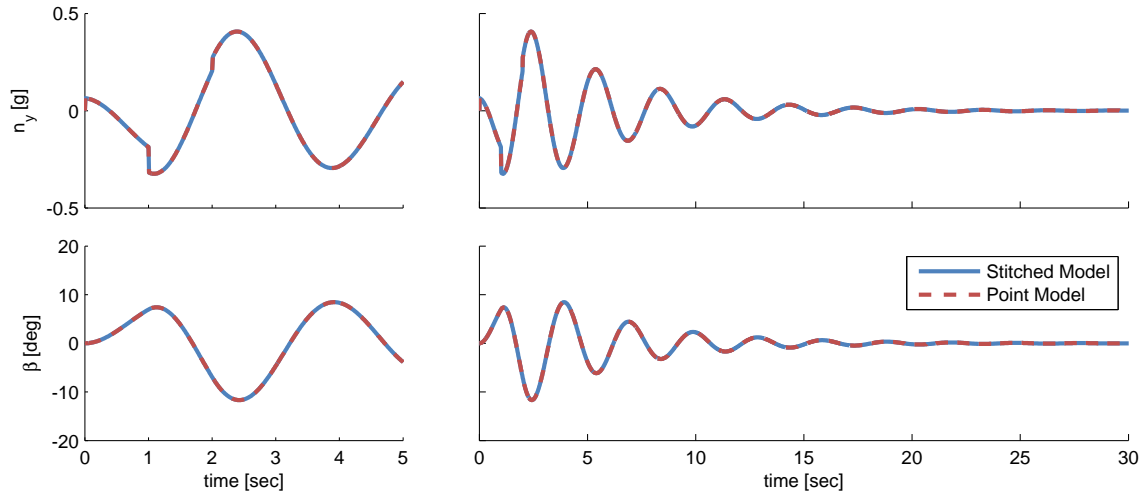


Figure 21. Check case: short- and long-term time history responses, rudder doublet.

## B. Piloted Frequency Sweeps

Separate control column, wheel, and pedal piloted frequency sweeps were performed in the simulator to verify the end-to-end response of the CJ1 stitched model. The simulation flight condition and loading configuration at which the sweeps were performed was 180 KTAS, 5000 ft altitude, and 9750 lb gross weight, which represented a flight condition and loading configuration of the aircraft flown in the piloted evaluations. Multiple sweep runs were performed for each control input, and each sweep was approximately 120 seconds in length. The sweep data were processed using CIPHER<sup>®</sup>,<sup>1</sup> and frequency responses were generated for key longitudinal and lateral/directional responses.

Figures 22–25 present the frequency responses from the piloted sweeps, which are compared with responses of the AAA truth point model. The coherence is very high over the entire frequency range of interest, indicating excellent identification accuracy and linearity of the responses. Results of the linearized stitched model are shown for reference. Overall there is excellent agreement between the results of the piloted sweeps, linearized stitched model, and truth point model.

## C. Time Delay Quantification

In order to ensure good simulation fidelity, it is important to measure the time delays inherent in the simulator hardware. Key time delay sources include the inceptors, computational delay, and visual processing delay in the rendering of the out-the-window visual scene by the projectors. In this study, a measurement of the total lumped delay  $\tau_{\text{sim}}$  was made by first modifying the stitched model to output aircraft attitude proportional to inceptor position (with no dynamics or internal model delays). Then, high speed (60 frames per second) video of rapid inceptor pulses was recorded with the inceptor, visuals, and a stopwatch in the frame of the shot. The recorded video was advanced frame by frame, and the time difference between the moment at which the inceptor first moved to when the aircraft attitude in the visuals first responded was used to estimate the total time delay, with an error of plus or minus half a video frame:

$$\tau_{\text{sim}} = 0.05 \pm 0.008 \text{ sec} \quad (30)$$

This overall time delay value of about 50 msec is well under the suggested threshold value of 120 msec,<sup>13</sup> therefore indicating that handling qualities will be unaffected by the simulator time delay.

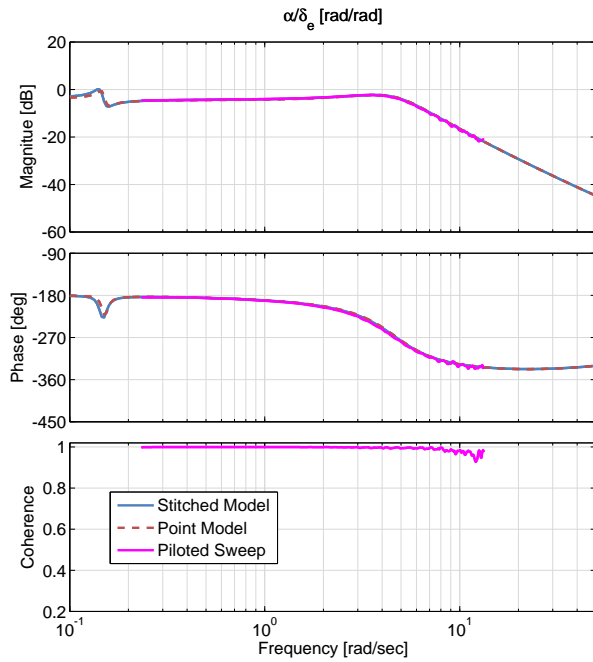


Figure 22. Piloted sweeps: angle-of-attack response to elevator input comparison.

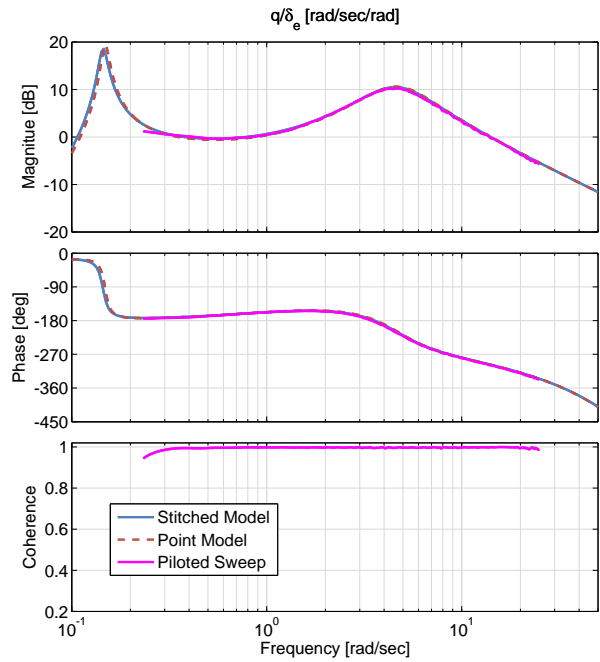


Figure 23. Piloted sweeps: pitch rate response to elevator input comparison.

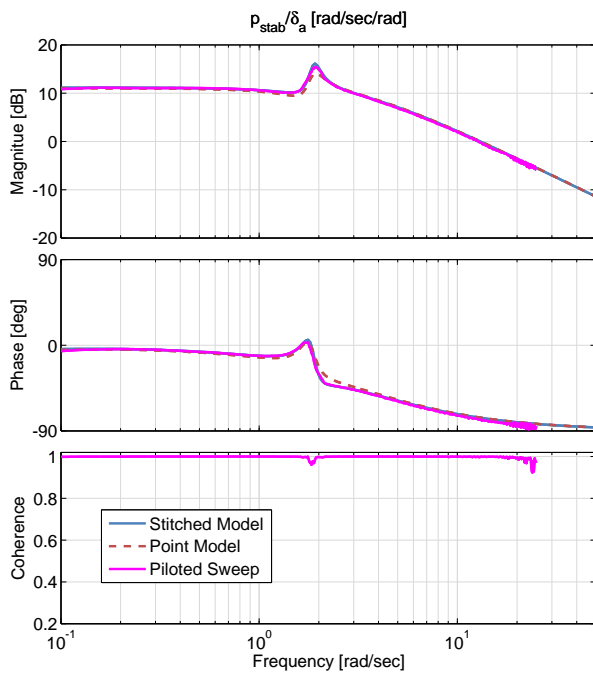


Figure 24. Piloted sweeps: roll rate response to aileron input comparison.

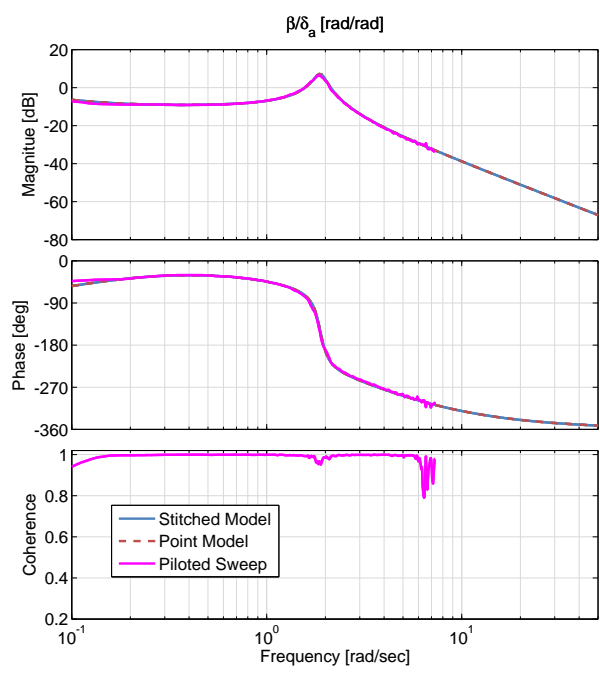


Figure 25. Piloted sweeps: sideslip response to aileron input comparison.

## V. Qualitative Evaluation Tasks

In preparation for the piloted evaluations, qualitative tasks were developed and refined. The short-term dynamic response of the stitched simulation model at any anchor point will be preserved, as demonstrated by the frequency response comparisons presented in Section IV. Therefore, tasks were designed to exercise continuous transition from one flight condition to another with variations in airspeed, altitude, and flap setting. The selected qualitative tasks include a level acceleration/deceleration, climbing s-turn, and simulated approach. The target task parameters and performance standards were developed with the pilots to ensure representative performance for the aircraft and to observe operating limitations in flight. Descriptions and performance standards for these tasks will be presented over Sections V.A–C.

### A. Level Acceleration/Deceleration

The level acceleration/deceleration or *accel/decel* task evaluates continuous changes in airspeed, covering a large portion of the airspeed envelope for the clean (flaps up and gear up) configuration. This task was performed at two altitudes; 5500 ft and 12,500 ft. Overall true airspeed ranges for this maneuver are approximately 150–270 KTAS at 5500 ft and 168–312 KTAS at 12,500 ft. Values of the target calibrated airspeeds are provided in Table 4. Performance standards for the maneuver are shown in Table 5.

From steady level flight at airspeed  $V_0$ , a level acceleration is initiated by increasing power to climb power; altitude and heading are maintained during the acceleration. The acceleration continues until the target high airspeed  $V_{\text{high}}$  is reached, at which point airspeed is captured and maintained within the specified tolerance for 10 seconds. Next, a level deceleration is initiated by reducing power to idle. The deceleration continues until the target low airspeed  $V_{\text{low}}$  is reached, at which point airspeed is captured and maintained within the specified tolerance for 10 seconds. Altitude and heading are to be tightly maintained during the entire maneuver. Pitch attitude is to be adjusted as required to meet the performance requirements of this maneuver. Power may be adjusted to capture the target airspeeds. No configuration changes (i.e., flap adjustments) are to be made during the maneuver.

Table 4. Target airspeeds – level acceleration/deceleration

| Variation | Altitude [ft] | $V_0$ [KCAS] | $V_{\text{high}}$ [KCAS] | $V_{\text{low}}$ [KCAS] |
|-----------|---------------|--------------|--------------------------|-------------------------|
| 1         | 5500 ft       | 200          | 250                      | 140                     |
| 2         | 12,500 ft     | 200          | 260                      | 140                     |

Table 5. Performance standards – level acceleration/deceleration

|  | Desired | Adequate |
|--|---------|----------|
| • X knots deviation from target airspeed | ±5 kn   | ±10 kn   |
| • X feet altitude deviation              | ±50 ft  | ±100 ft  |
| • X degrees heading deviation            | ±2 deg  | ±5 deg   |

### B. Climbing S-Turn

The *climbing s-turn*<sup>14</sup> task incorporates continuous changes in altitude and heading at a constant calibrated airspeed. Two variations of this maneuver were performed; one in a climb, and the other in a descent. Overall altitude ranges for this maneuver are approximately 5500–10,500 ft in the climbing s-turn, and 12,500–6500 ft in the descending s-turn. Values of the target calibrated airspeeds and altitudes are provided in Table 6. Performance standards for the maneuver are shown in Table 7.

From steady level flight at altitude  $h_1$ , climb power is set, and a climbing left turn is initiated with a target 20-degree bank angle, steady airspeed  $V_0$ , and reasonable climb rate. Once the left turn has progressed through 90 degrees, a climbing right turn with 20-degree bank angle is initiated. Steady airspeed  $V_0$  and reasonable climb rate are maintained until right turn has progressed through 90 degrees, at which point the aircraft is leveled off at altitude  $h_2$  to return to the initial heading. Steady conditions are maintained for a minimum of 15 seconds.

The maneuver is repeated in a descent, which is referred to as a *descending s-turn*. Vertical speed is naturally somewhat greater in the descending s-turn as compared to the climbing s-turn, so a larger range of altitude is covered in approximately the same length of time.

**Table 6. Target parameters – climbing s-turn**

| Variation  | $V_0$ [KCAS] | Altitude Range ( $h_1-h_2$ ) [ft] |
|------------|--------------|-----------------------------------|
| Climbing   | 220          | ~5500–10,500                      |
| Descending | 250          | ~12,500–6500                      |

**Table 7. Performance standards – climbing s-turn**

|  | Desired | Adequate |
|--|---------|----------|
| • X degrees deviation from target bank angle | ±2 deg  | ±5 deg   |
| • X degrees deviation in final heading       | ±2 deg  | ±5 deg   |
| • X knots deviation in airspeed              | ±10 kts | ±15 kts  |

### C. Simulated Approach

The *simulated approach* task mimics the sub-phases of an approach to landing, including power and flap adjustments, gear extension, and capturing a descent rate, and is performed in an up-and-away flight condition. The aircraft transitions from a clean (flaps and gear up) configuration to a landing (full flaps, gear extended) configuration throughout the maneuver, covering a true airspeed range of 125–223 KTAS. Target calibrated airspeeds and altitudes are shown in Table 8. Performance standards for the maneuver are provided in Table 9.

From steady level flight at airspeed  $V_0$  and altitude  $h_1$  in a clean configuration, power is reduced to initiate a deceleration, and a 15-degree flap deflection is selected while altitude and heading are maintained. Continuing through the deceleration, landing gear are extended at  $V_{LE}$ , and a 35-degree flap deflection is selected at  $V_{FE}$ . A descent rate of 600–800 ft/min is targeted while airspeed converges on the landing reference airspeed  $V_{Ref}$ . The aircraft is leveled off at altitude  $h_2$ , and steady conditions are maintained for 15 seconds.

**Table 8. Target parameters – simulated approach**

| $V_0$ [KCAS] | $V_{LE}$ [KCAS] | $V_{FE}$ [KCAS] | $V_{Ref}$ [KCAS] | Altitude Range ( $h_1-h_2$ ) [ft] |
|--------------|-----------------|-----------------|------------------|-----------------------------------|
| 200          | ~185            | ~160            | ~115             | ~7500–6000                        |

**Table 9. Performance standards – simulated approach**

|   | Desired | Adequate |
|---|---------|----------|
| • X knots deviation from target airspeed $V_{Ref}$        | ±5 kn   | ±10 kn   |
| • X feet altitude deviation from level-off altitude $h_2$ | ±50 ft  | ±100 ft  |
| • X degrees heading deviation                             | ±2 deg  | ±5 deg   |

## VI. Results of Piloted Fidelity Assessment

Back-to-back flight/simulation piloted evaluations involving a light business jet in flight and the CJ1 stitched model in Cessna’s fixed-base simulator facility were performed by two Cessna engineering test pilots to assess the qualitative fidelity of the stitched model. Qualitative tasks, as presented in Section V, were selected to exercise continuous transition between flight conditions with variations in airspeed, altitude, and flap setting.

A 2-hour evaluation flight in a light business jet was conducted by the two evaluation pilots (Pilot A and Pilot B) in which each pilot performed all qualitative tasks sequentially as outlined in Table 10. Task performance was monitored by the co-pilot during each evaluation run. Upon completion of the maneuver the co-pilot reported on the overall performance values obtained, and noted specific deviations, if applicable.

Performance standards for the task were referenced, and it was determined whether Desired or Adequate performance was met. After completion of each task, the pilot questionnaire (Appendix A) was administered by the flight test engineer over the intercom. As part of the questionnaire, the pilot assigned ratings for Precision (Figure A.1) and Predictability (question #9). Pilots had the opportunity to comment and take notes on control strategy, aircraft response, etc. during the evaluation.

After a short recess following the flight evaluation, the pilots repeated the qualitative tasks in the Cessna fixed-base simulator facility. The tasks were evaluated in the same order in which they were performed in flight. Furthermore, because inceptors were installed in both left- and right-seat positions, the pilots were able to sit in the same cockpit position in which they flew in the aircraft. As in flight, task performance was monitored by the co-pilot, and it was determined whether Desired or Adequate performance was met. The pilot questionnaire was again administered after completion of each task, and the evaluation pilot assigned Precision and Predictability ratings. Additionally, the evaluation pilot utilized the Simulation Fidelity Rating scale to quantify simulation fidelity for each evaluation task.

The Simulation Fidelity Rating (SFR) scale, as developed by Perfect et al.,<sup>3</sup> is shown in Figure A.2 in Appendix A. The organizational structure and semantics of the SFR scale have been adopted from the Cooper-Harper Handling Qualities Rating<sup>15</sup> (HQR) scale. In the SFR scale, comparative task performance and task strategy adaptation between flight and simulation are considered for the evaluated task. The evaluation pilot works through the decision tree to arrive at a Simulation Fidelity Rating, while providing justification for the rating. Akin to the HQR scale, Simulation Fidelity Ratings are divided into Fidelity Levels (e.g., Level 1, Level 2, etc.) where Fidelity Level 1 suggests that the simulation is “fit for purpose” with “full transfer of training for the selected task,” and where Fidelity Level 2 suggests that “fidelity warrants improvement” with “limited transfer of training for the selected task.”

Sections VI.A–C present the qualitative and quantitative results from flight and simulation, covering the entire piloted fidelity assessment. Results are grouped by task, in which the achieved performance, assigned ratings, and corresponding justifications are presented for both evaluation pilots.

**Table 10. Evaluation test points**

| # | Task               | Variation  |
|---|--------------------|------------|
| 1 | Level Accel/Decel  | 5500 ft    |
| 2 | S-Turn             | Climbing   |
| 3 | Level Accel/Decel  | 12,500 ft  |
| 4 | S-Turn             | Descending |
| 5 | Simulated Approach |            |

### A. Level Acceleration/Deceleration

The level accel/decel task, as described in Section V.A, was performed at two altitudes: 5500 ft and 12,500 ft. The level accel/decel task at 5500 ft was the first evaluated task of the flight. Precision, Predictability, and Simulation Fidelity ratings for the level accel/decel task at an altitude of 5500 ft are summarized in Figure 26.

In Pilot A’s flight evaluation, altitude was kept just within the desired  $\pm 50$ -ft limit, airspeed was slightly overshoot by 2 knots for both high/low target airspeeds, and heading was kept within  $\pm 4$  deg, for overall Desired performance. A Precision rating of 1 was assigned. A Predictability rating of 2 was given because of the slight airspeed overshoot due to throttle inputs. Overall control strategy for the task involved controlling pitch attitude to maintain altitude, and adjusting throttle to capture airspeed.

In Pilot B’s flight evaluation, altitude was maintained within  $\pm 30$  feet, heading within  $\pm 3$  deg, and airspeed was undershot by about 3 knots at the high airspeed, for Desired performance. A Precision rating of 1 was assigned. Pilot B also gave a Predictability rating of 2 due to the slight unpredictability of throttle inputs. Pilot B’s general control strategy was the same as that reported by Pilot A, and added that his “primary scan was on altitude” and cross-referenced the other parameters.

Performance values of Pilot A in simulation were similar to those in flight, with airspeed overshoots of about 3 knots on the high target airspeed and 4 knots on the low target airspeed, for overall Desired performance. A Precision rating of 2 (“slightly less than optimal”) was assigned in simulation because of the difficulty of maintaining altitude due to the simulator’s altimeter display (see discussion in Section VII.A).

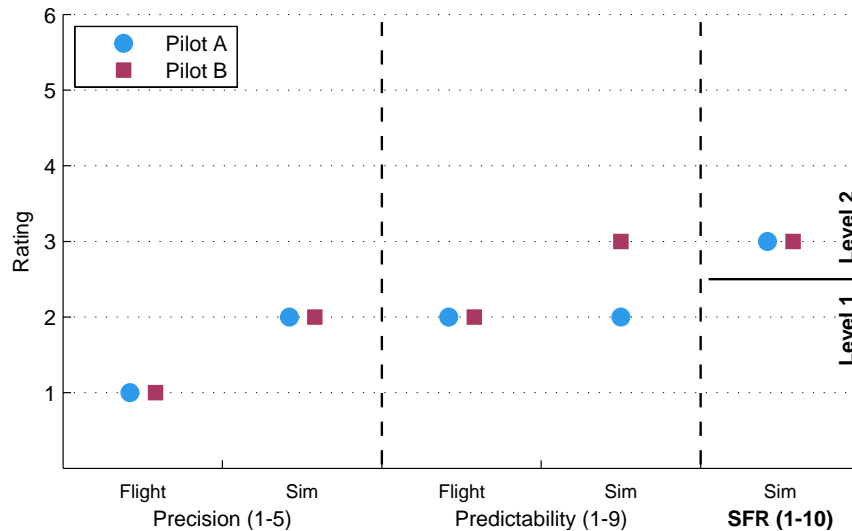


Figure 26. Pilot ratings – level accel/decel, 5500 ft.

Predictability was rated a 2 as in flight due to uncertainty in throttle inputs for airspeed capture. Pilot A further noted that the throttle seemed “a bit more responsive” in the simulator. As a general comment, he noted that “the [inceptor] forces felt pretty much like they should.” With the amount of airspeed overshoot being slightly greater in simulation as compared to flight (similar performance), and minimal adaptation of task strategy required, Pilot A assigned an SFR of 3 for this task. This SFR is just within Fidelity Level 2, suggesting “fidelity warrants improvement” for this task.

Pilot B’s performance in simulation was Desired and similar to that in flight, however airspeed was overshoot by about 5 knots for both targets, which contrasts the undershoot reported in flight for the high airspeed target. He noted more sensitivity in roll, for a Precision rating of 2. He commented that “everything responded the way I expected it to... it was just the magnitude that was a little different sometimes,” for a Predictability rating of 3. With similar performance attained and minimal strategy adaptation due to higher control input gains required, an SFR of 3 was given, which is just within Fidelity Level 2.

The level accel/decel was repeated at an altitude of 12,500 ft in flight. Aside from the difference in altitude, the high airspeed target  $V_{high}$  was 260 KCAS as opposed to 250 KCAS, as shown in Table 4. A summary of the Precision, Predictability, and Simulation Fidelity ratings for the level accel/decel task at an altitude of 12,500 ft is given in Figure 27.

Pilot A achieved comparable flight performance to that of his evaluation at 5500 ft, with overall Desired performance. His Precision rating of 1 and Predictability rating of 2 matched those from his 5500-ft evaluation, again stating he overshoot on the throttle a bit, and added that throttle “required a little hunting” to tightly capture the target airspeeds. Overall control strategy was noted to be the same as that of the 5500-ft run.

Pilot B had very similar flight performance compared to his 5500-ft run, with altitude maintained within  $\pm 40$  feet, heading within  $\pm 2$  deg, and airspeed overshoot by about 2 knots, for Desired performance. As with Pilot A, Pilot B gave the same ratings for both his 5500-ft and 12,500-ft evaluations; Precision rating of 1, and Predictability rating of 2.

In simulation, Pilot A achieved equivalent Desired performance to that of his flight evaluation. A Precision rating of 1 (“optimal”) and a Predictability rating of 2 were given, which were the same ratings given in flight. With equivalent performance and only minimal adaptation of strategy required, an SFR of 2 was assigned to this task. This SFR is within the best Fidelity Level, Level 1, which suggests the simulation is “fit for purpose” for this level accel/decel task, and also suggests “full transfer of training” for this task.

Pilot B in simulation had equivalent performance to his flight evaluation, with altitude held within  $\pm 40$  ft and heading kept within  $\pm 3$  deg, but commented that it was “a little more difficult to achieve Desired performance” in simulation because he had to increase his rate of scan and level of attention. He gave a Precision rating of 1 and a Predictability rating of 2, which were the same ratings given in flight. He

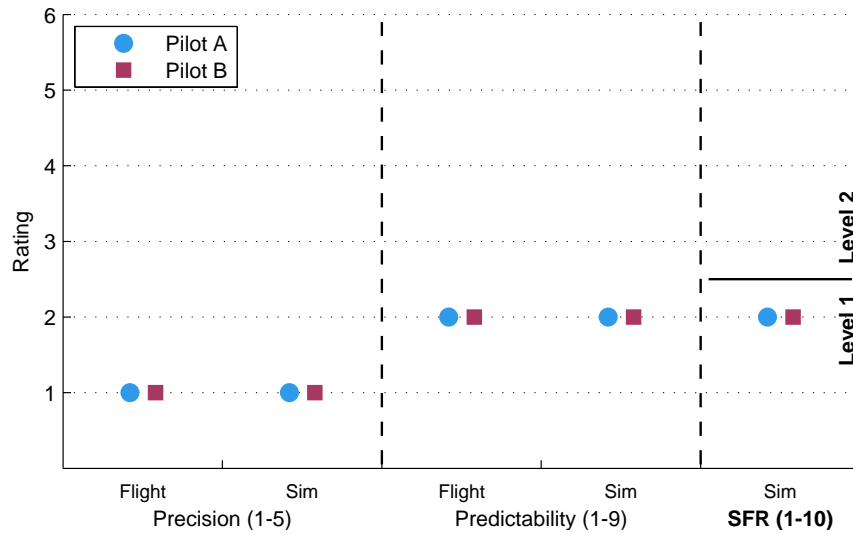


Figure 27. Pilot ratings – level accel/decel, 12,500 ft.

elaborated on the predictability of the simulation model saying that “all the initial responses were predictable, and in line with normal behavior,” and “the predictability was very similar to the airplane... with everything I did I got the response that I wanted out of it.” Equivalent task performance and a minimal adaptation of task strategy due to increased rate of scan yielded an SFR of 2. Again, this SFR is within Fidelity Level 1, suggesting “full transfer of training” for this task.

## B. S-Turn

The climbing s-turn and descending s-turn tasks, as described in Section V.B, were performed. Figure 28 provides a summary of the Precision, Predictability, and Simulation Fidelity ratings assigned for the climbing s-turn task.

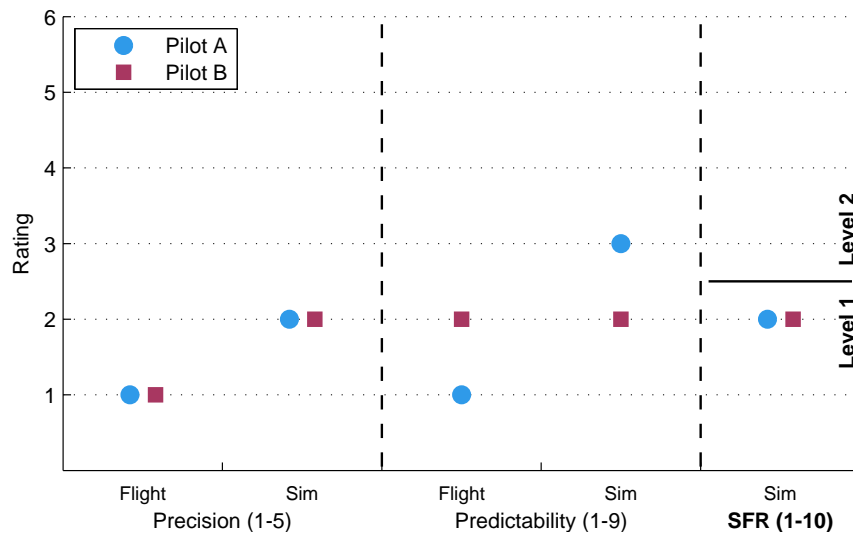


Figure 28. Pilot ratings – climbing s-turn.

Pilot A initiated the climbing s-turn from an altitude of 5500 ft and a South heading in flight. He maintained the target 20-deg bank angles within  $\pm 3$  deg during the left and right turns, kept airspeed within  $\pm 10$  knots throughout, and captured the initial South heading at the conclusion of the run, for overall

Desired performance. Although not a specific part of the performance criteria, the targeted altitude of 10,500 ft was overshoot by about 50 ft when leveling off, which the pilot initiated 300 ft below the target altitude. Considering the airspeed, bank angle, and heading criteria, a Precision rating of 1 and a Predictability rating of 1 were assigned. Pilot A’s overall control strategy involved targeting a pitch attitude that maintained airspeed, and he referenced the 20-deg “tick mark” on the display in order to maintain roll attitude.

Flight performance for Pilot B was also Desired: airspeed was tightly maintained within  $\pm 1$  knot throughout, bank angles were held within  $\pm 1$  deg, and the final heading was precisely converged upon. Like Pilot A, Pilot B overshoot the intended level-off altitude of 10,500 ft by about 40 ft. Precision was rated 1, whereas Predictability was rated 2 because “more pitch control than expected was needed when increasing power.” His overall control strategy was similar to Pilot A’s, and noted that he primarily focused on maintaining airspeed.

In simulation, Pilot A maintained airspeed within 9 knots, kept bank angle within  $\pm 2$  deg, and precisely captured the final heading, for Desired performance. He noted he “paid more attention to altitude” to closely capture the intended level-off altitude. He also noted that “roll attitude was a bit harder to control” as compared to flight, which led him to give a Precision rating of 2 and a Predictability rating of 3. He stated that the predictability of the initial aircraft responses were “good.” Equivalent task performance with minimal strategy adaptation resulted in the assigned SFR of 2. An SFR of 2 is within Fidelity Level 1, which suggests “full transfer of training” from simulation to actual aircraft for this climbing s-turn task.

Pilot B’s simulation performance was equivalent to his Desired performance in flight, with airspeed on the initial climb slightly under target by about 5 knots. He stated that this task overall was “similar to the airplane.” Like Pilot A, Pilot B also commented on the roll axis, saying he “needed to pay more attention to roll” compared to flight, and he “had to make small-gain roll corrections” to maintain bank angle. Precision was “very close to optimal,” for a Precision rating of 2, and Predictability was also rated a 2. With equivalent performance attained, and minimal adaptation of strategy due to greater attention needed on bank angle, an SFR of 2 was given, which is within Fidelity Level 1.

The s-turn was performed also in a descent, which is referred to as the descending s-turn task. Precision, Predictability, and Simulation Fidelity ratings for the descending s-turn task are summarized in Figure 29.

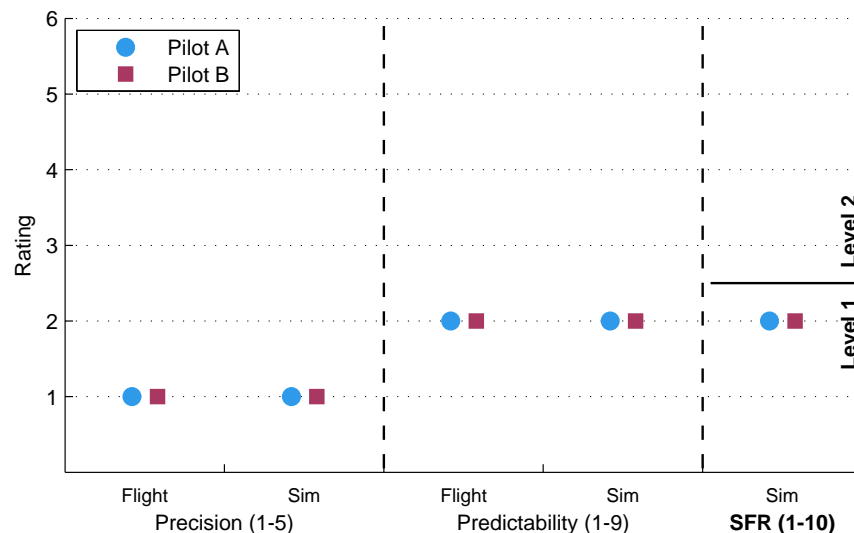


**Figure 29. Pilot ratings – descending s-turn.**

In flight, Pilot A met all Desired performance criteria in the descending s-turn. An altitude of 7000 ft was captured while rolling-out on a North heading. Precision was rated a 1 while Predictability was rated a 2 due to slight unpredictability of necessary throttle inputs.

Pilot B’s flight evaluation yielded Desired performance, with airspeed maintained within  $\pm 3$  knots. The initial bank into the right turn was briefly overshoot by about 4 deg. A level-off altitude of 6500 ft was targeted and captured within 40 ft. He commented that he had his “hands off the yoke a bit in the left turn and everything was stable for 10 seconds.” A Precision rating of 1 and a Predictability rating of 2 were given.

Pilot A in simulation met all Desired performance criteria for the descending s-turn, with airspeed maintained within  $\pm 3$  knots throughout. He commented saying “the descent looks reasonable” and noted again the extra attention needed in the roll axis to hold bank angle. He gave this task in simulation a Precision rating of 1 and a Predictability rating of 2. Because equivalent performance was attainable, but more attention was necessary on the roll axis, an SFR of 2 was assigned. This rating is in Fidelity Level 1, which indicates the simulation is “fit for purpose” for performing the descending s-turn task.

Pilot B met all Desired performance criteria in the simulator, as well. During the descent, he had his hands off the controls for a few seconds and noted it was trimmed and stable, as it was in flight. However, he noted he still needed to make “minor roll inputs to correct for bank angle” during portions of the maneuver. A Precision rating of 1 and a Predictability rating of 2 (“very predictable”) were given. With equivalent Desired performance attained, and minimal adaptation of strategy due to required roll inputs, he gave this task an SFR of 2 (Fidelity Level 1).

### C. Simulated Approach

The simulated approach task, as described in Section V.C, contains the sub-phases of an approach to landing, but is performed in an up-and-away flight condition. A summary of the Precision, Predictability, and Simulation Fidelity ratings for the Simulated Approach task is given in Figure 30.

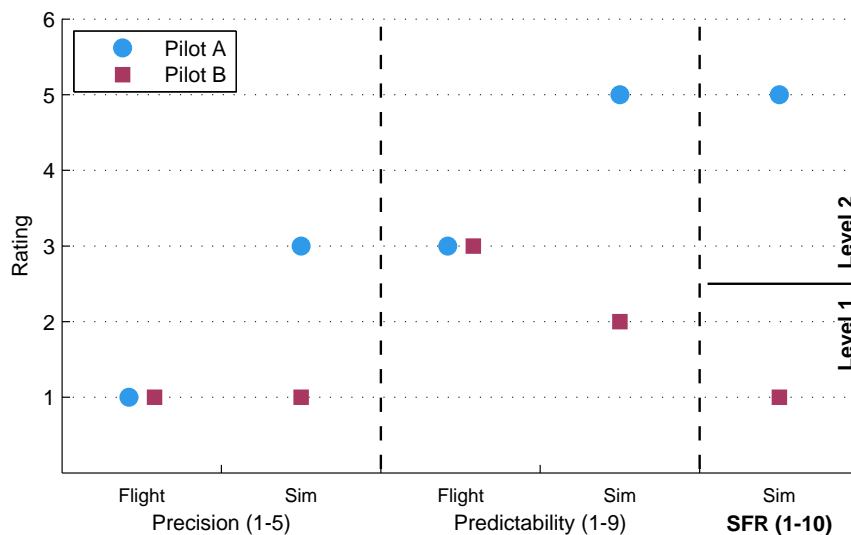


Figure 30. Pilot ratings – simulated approach.

In the flight evaluation, Pilot A tracked airspeed within  $\pm 5$  knots, heading was held within  $\pm 5$  deg, and the level-off altitude was maintained within about  $\pm 50$  ft, for borderline Desired performance overall. He commented that the lack of visual cues in the up-and-away flight condition made altitude “difficult to maintain” and added “the level off is not normal... there are more cues at the runway.” He rated Precision a 1 and Predictability a 3 because of the difficulty in maintaining altitude.

Pilot B achieved overall Desired performance in flight, with airspeed tracked within  $\pm 2$  knots, heading held within  $\pm 3$  deg, and level-off altitude captured within  $\pm 40$  ft. Upon deployment of 15-deg flaps, he noted a “fairly good push” on the control column was required to hold altitude, and that it was “more push than anticipated”. He added that no push or pull on the control column was necessary to hold altitude for deployment of 35-deg flaps. He gave a Precision rating of 1 and a Predictability rating of 3 because of the control force required for 15-deg flaps.

In simulation, Pilot A achieved similar performance compared to his flight evaluation, with overall Desired performance. His comments mostly focused on the amount of control compensation and control force required upon deployment of 15- and 35-deg flaps. For deployment of 15-deg flaps, he stated he needed to put in “a much bigger push than in the airplane” to hold altitude, and said “more throttle compensation was required at full [35-deg] flaps” to maintain airspeed. He gave this task in simulation a Precision rating of 3 because of the compensation required with flaps, and a Predictability rating of 5 for the same reasons. Although

similar performance was attainable in the simulator, he felt it was a “moderate adaptation of task strategy,” resulting in an SFR of 5. This SFR is solidly within Fidelity Level 2, indicating that more work is needed to improve simulation fidelity for deployment of flaps for Pilot A.

Pilot B’s simulation evaluation was comparable to his flight evaluation, with overall Desired performance met; airspeed tracking was within 2 knots and level-off altitude was captured and maintained within  $\pm 40$  ft. In contrast to Pilot A, Pilot B stated that the control force required upon deployment of 15-deg flaps “felt slightly lighter in the sim.” He gave a Precision rating of 1 and a Predictability rating of 2, adding that the simulation model response to piloted inputs was “very predictable” and “it was actually very similar to the airplane.” Equivalent task performance was attained with “negligible or less adaptation of task strategy,” for an SFR of 1. This is the best Simulation Fidelity Rating possible, and is solidly within Fidelity Level 1, indicating “full transfer of training” from simulation to actual aircraft for this simulated approach task.

## VII. Discussion

This section covers discussions on findings and lessons learned about the piloted fidelity assessment and the assigned ratings, the simulation environment, and use of the Simulation Fidelity Rating scale. Guidance on future flight testing for the development of fixed-wing aircraft stitched models is also provided.

### A. Simulation Environment

This section presents discussions on aspects of the simulator and overall simulation environment that potentially impacted pilot perception of the CJ1 stitched simulation model. Topics include pilot cues, inceptor loader characteristics, control wheel friction, and representative engine model.

As simulation evaluations were conducted in a fixed-base simulator facility, pilot cues were expectedly limited. The lack of motion cues especially impair pilot perception of aircraft acceleration. In the level accel/decel task, for example, the pilots did not have longitudinal acceleration cues in simulation as they did in flight. This lack of lead feedback to the pilots likely contributed to the overshoots in throttle setting during airspeed capture, as noted for Pilot A’s simulation evaluation of the accel/decel task at 5500 ft (Section VI.A), and also likely contributed to the increased rate of scan and higher level of attention noted by Pilot B for the same task at 12,500 ft.

The inceptor loader models in the simulator were based on a similar aircraft model as the CJ1, and tuned by experienced CJ1 pilots to match the in-flight force-response relationship. In general, the pilots noted that the control column, wheel, and pedal controller forces in the simulator were representative of the aircraft. During Pilot A’s simulation evaluation of the level accel/decel task at 5500 ft (Section VI.A), he commented that the inceptor forces “felt pretty much like they should.”

The modeled friction of the control wheel in the simulator was tuned to the on-ground value of the representative aircraft. In the flight evaluations, the actual aircraft control wheel demonstrated nearly zero friction due to the aerodynamic forces and turbulence on the control surfaces. As a result, the aircraft control wheel easily returned to the trimmed position when the pilot forces were removed. In contrast, the simulator control wheel did not exactly return to its trimmed position when the pilot forces were removed due to the effective hysteresis induced by the modeled friction, resulting in small aileron inputs to the simulation model. This manifested as a perceived roll sensitivity issue, on which both pilots commented during their simulation evaluations. One example was during Pilot B’s evaluation of the climbing s-turn (Section VI.B) in which he stated that he “had to make small-gain roll corrections” to maintain bank angle.

A simple engine model (Section III.D.2) was employed in the stitched simulation model, with representative maximum and idle thrust values looked-up as functions of altitude and Mach, and a second-order representation of engine response dynamics. On a few occasions the pilots commented on the similarities or slight differences in the power setting (expressed as % N1) for a particular trim flight condition in simulation as compared to what they had noted in the aircraft. In general the values were very close considering only a representative engine model. However, at times when the pilots were tightly in the loop with throttle, the representative engine model in simulation likely contributed to comments about throttle sensitivity (Section VI.A, level accel/decel, 5500 ft, Pilot A) and performance in airspeed capture (Section VI.A, level accel/decel, 5500 ft, Pilot B).

After completion of the first task evaluation in the simulator, the pilot commented that the type of altimeter display was slightly different than the one in the aircraft. The altimeter display in the aircraft had

a rolling marker, so that motion within a 20-ft band was known. However, in the simulator, the altimeter’s digital output only changed indication to a 20-ft resolution, which caused a deadband in the visual feedback to the pilot. This made capturing and holding altitude more difficult. An improved visual display that better matches the aircraft avionics would include a rolling altimeter “barrel” so that motion within the 20-ft indication could be discerned.

## **B. CJ1 Stitched Simulation Model**

The CJ1 stitched simulation model well represented the aircraft for the evaluated tasks, which exercised continuous variations in airspeed, altitude, and flap setting covering a significant portion of the flight envelope. The qualitative tasks overall covered approximately 5000 ft through 13,000 ft in altitude, true airspeeds of approximately 150–315 KTAS in a clean (flaps and gear up) configuration, and a true airspeed as low as approximately 125 KTAS in the landing (full flaps, gear extended) configuration. Additionally, a true airspeed of 330 KTAS at 15,000 ft altitude, which is close to the maximum operating limit, was evaluated during a set of piloted frequency sweeps. The frequency responses as obtained from the sweep results were verified against the corresponding AAA truth model, showing excellent match.

Pilot comments on the fidelity of the stitched model for the evaluations performed in simulation were generally quite positive. For the level accel/decel task, Pilot A commented that “the [inceptor] forces felt pretty much like they should,” and Pilot B said “everything responded the way I expected it to.” In the climbing s-turn task, Pilot B stated that precision was “very close to optimal,” and Pilot A in the descending s-turn commented that “the descent looks reasonable.” As for the simulated approach task, Pilot B noted that the simulation model response to piloted inputs was “very predictable” and “it was actually very similar to the airplane.”

Overall impressions were that the stitched simulation model was representative of the actual aircraft. Pilot A felt “it was representative for the tasks performed.” Pilot B stated that “the basic, overall flying qualities are represented well.”

## **C. Use of Simulation Fidelity Rating Scale**

The Simulation Fidelity Rating<sup>3</sup> (SFR) scale, as shown in Figure A.2, was used to quantify the fidelity of the CJ1 stitched model for the selected qualitative tasks. The utilization of the SFR scale itself, and associated test planning, task selection, and pilot briefing, was done in accordance with guidance provided by the authors of the scale.

Upon completion of each task in simulation, the evaluation pilot’s performance values were stated aloud by the co-pilot, and his corresponding performance values from flight were reiterated to determine the degree of comparative task performance. Desired performance was attained for most parameters in both flight and simulation evaluations, so the degree to which Desired performance was met (e.g., tightness of airspeed tracking or amount of overshoot) was considered to distinguish between “equivalent” and “similar” task performance.

The degree of task strategy adaptation was somewhat more subjective, and the justifications given varied between pilots and tasks. A “minimal adaptation of task strategy” was chosen most frequently; however, during the evaluation of the simulated approach task (Section VI.C), the assessed force of the control compensation required to maintain altitude during deployment of flaps was dissimilar between pilots, resulting in Pilot A’s “moderate adaptation of task strategy” and Pilot B’s “negligible or less adaptation of task strategy.” Overall, the SFR scale was effective at quantifying simulation fidelity for particular aspects of specific tasks.

## **D. Flight Test Implications for Development of a Fixed-Wing Aircraft Stitched Model**

A key application of the model stitching architecture is the development of full flight-envelope stitched simulation models from flight-identified point models using system identification methods<sup>1</sup> and associated flight-test trim data. The extrapolation methods employed in the model stitching architecture permit continuous, full flight-envelope simulation of a full range of aircraft loading configurations using only a small number of point models and trim points. This key aspect significantly reduces required flight test points, which directly reduces the associated flight time, cost, and analysis effort.

A suitably-instrumented aircraft is required for data collection, with level of instrumentation dictated by the desired model complexity and choice of states. A frequency-domain-based approach of system identification is suggested, which involves performing piloted or automated frequency sweeps in the primary axes and processing the collected flight-test data in CIPHER<sup>®</sup>.<sup>1</sup> See Tischler<sup>1</sup> for detailed discussions on the collection of flight-test data, including instrumentation requirements, pilot input methods, and guidelines on record duration.

This section covers the overall considerations for planning a flight test involving fixed-wing aircraft for the development of stitched simulation models. Analyses of the fixed-wing data trends presented herein and lessons learned are applied to provide guidance on the spacing and quantity of trim data points and point models, suggested test altitudes, and required aircraft configurations. A summary of the overall flight test recommendations is provided in Table 11.

### 1. Data Collection Process

Discussed below are the suggested guidelines for the collection of all necessary trim points and identification point models.

**TRIM DATA** The collection of trim data is accomplished by trimming the aircraft at the desired flight condition and recording data for a duration of approximately 3–5 seconds. Post-flight processing of the data is conducted to determine the trim values of the controls, aircraft attitude, and any additional states for the particular flight-test point.

It is important to capture critical inflections in trim curves (e.g., bottom of the power curve, Mach effects, etc.) for accurate simulation over the airspeed envelope. Collecting trim data at finely-spaced speed increments (e.g., every 30–50 knots) over the entire airspeed range should ensure capture of the key trim trends. Finer spacing of trim may be needed at the critical inflections for accurate determination of speed derivatives. Prior knowledge of the aircraft response behavior over specific airspeed ranges may allow trim to be collected at coarser speed increments (e.g., every 50 knots) between such regions, necessitating finer increments for the critical regions only.

**IDENTIFICATION POINT MODELS** The process of identifying point models involves performing frequency sweeps in each primary axis at a particular flight condition. This process is more time consuming and involves both flight testing and identification analysis efforts, so careful consideration of the required identification points is critical.

Through analyses of stability and control derivative trends over ranges of airspeed, it has been determined that 4 identified point models are sufficient to accurately represent the dynamic response of the fixed-wing aircraft over the entire airspeed range for a particular altitude. This guidance is applicable to both dimensional and nondimensional derivatives. The 4 identification points may be roughly evenly spaced over the airspeed range. To accurately capture variations in stability and control derivatives due to Mach effects, it is suggested to more-closely space the identification points at the high-speed (Mach  $\geq 0.5$ ) regime.

### 2. Aircraft Configurations

The extrapolation methods integrated into the model stitching architecture were shown to very accurately simulate off-nominal values of weight and CG (Section III.E). Therefore, collecting trim data and identification models is necessary using only the nominal (baseline) aircraft loading configuration. If the modeling of flaps is desired, trim data alone may be collected at a few (2–3) flap settings and airspeeds to effectively model the principal flap deflection effects.

### 3. Altitude

Altitude extrapolation is accomplished within the model stitching architecture by scaling the dimensional stability and control derivatives and specific aerodynamic trim forces by the air density ratio ( $\rho_{\text{sim}}/\rho$ ) and retrimming the model, as discussed in Section II.E. This extrapolation method has been shown to be very accurate over 10,000 ft in altitude change, and reasonable results were found for greater altitude changes.

The operational service ceiling of the representative light business jet modeled herein is approximately 40,000 ft. Based on the applicable range for altitude extrapolation mentioned above, point linear models and trim data were generated at altitudes of 10,000 ft and 30,000 ft; the 10,000-ft data were extrapolated to

sea level (0 ft) and 20,000 ft, and the 30,000-ft data were extrapolated to 40,000 ft. With data at only two altitudes, the entire altitude envelope was effectively and accurately covered in 10,000-ft increments by the extrapolation method, as presented in Section III.C.

Flight testing at two altitudes is recommended to allow the extrapolation method to accurately cover the entire altitude envelope. This strategy of using data from two altitudes was demonstrated in the verification results presented in Section III.E.3. If flight testing at more than one altitude is cost prohibitive, data collected at a single altitude may be extrapolated to cover the entire flight envelope; however, certain trim and derivative trends may not be precisely captured.

**Table 11. Summary of flight test recommendations for development of fixed-wing aircraft stitched models**

| Interpolation Dimension | Parameter       | ID Models                          | Trim Data  |
|-------------------------|-----------------|------------------------------------|--|
| Airspeed                | Increment [kn]  | 80–100 <sup>a</sup>                | 30–50 <sup>b</sup>   |
|                         | # of airspeeds  | 4–6                                | 8–12   |
|                         | Example profile | [ <i>approach</i> 180 270 330 360] | [ <i>approach</i> 120 150 180 210 240 270 300 330 360 390] |
| Altitude                | Increment [ft]  | 20,000                             | 20,000   |
|                         | # of altitudes  | 1–2 <sup>c</sup>                   | 1–2 <sup>c</sup>   |
|                         | Example profile | [10,000 30,000]                    | [10,000 30,000]  |

<sup>a</sup> Finer increment at high speed (Mach  $\geq 0.5$ ) to capture nondimensional derivative variation due to Mach effects

<sup>b</sup> May need finer increment around critical inflections (e.g., bottom of the power curve)

<sup>c</sup> Two altitudes recommended for accurate altitude extrapolation

## VIII. Conclusions

1. The model stitching technique of combining linear point models and trim data for discrete flight conditions allows for accurate, continuous, full flight-envelope simulation of a business jet. Only a small number of linear point models over the airspeed range and at a nominal weight/CG are needed. More finely-spaced trim data are also needed to correctly capture trends and key inflections.
2. Linear point models and trim data at two altitudes provides for an accurate simulation of altitude effects using air density-ratio scaling. Additionally, accurate simulation of off-nominal loading configurations (i.e., variations in gross weight and CG location) is accomplished by real-time extrapolation within the model stitching architecture without the need for additional data.
3. Back-to-back flight/simulation evaluations allowed for the efficient assessment and quantification of simulation fidelity for the selected evaluation tasks based on pilot comments and Simulation Fidelity Ratings. The selected evaluation tasks effectively exercised the CJ1 stitched model in a continuous and realistic fashion for variations in airspeed, altitude, and flap setting.
4. Overall pilot impressions were that the stitched simulation model was representative of the actual aircraft, despite the limited cues in the fixed-base simulator, the use of a simple engine model, and the basic modeling of flap deflection effects. Mostly Level 1 Simulation Fidelity ratings were assigned to the stitched simulation model for the evaluated tasks, which suggests full transfer of training from simulation to actual aircraft for those tasks.

## Appendix A Pilot Questionnaire

### TASK PERFORMANCE

1. Describe ability to meet DESIRED / ADEQUATE performance standards.
2. Rate the level of precision. Use the Precision Rating Scale.
3. If trying for DESIRED performance resulted in unacceptable oscillations, did decreasing your goal to ADEQUATE performance alleviate the problem?

### AIRCRAFT CHARACTERISTICS

4. Describe predictability of initial aircraft response.
5. Describe any mid- to long-term response problems.
6. Describe any objectionable oscillations or tendency to overshoot.
7. Describe any non-linearity of response.
8. Describe any problems with harmony of pitch and roll, speed control, and turn coordination.
9. Rate the predictability of aircraft response to pilot inputs:

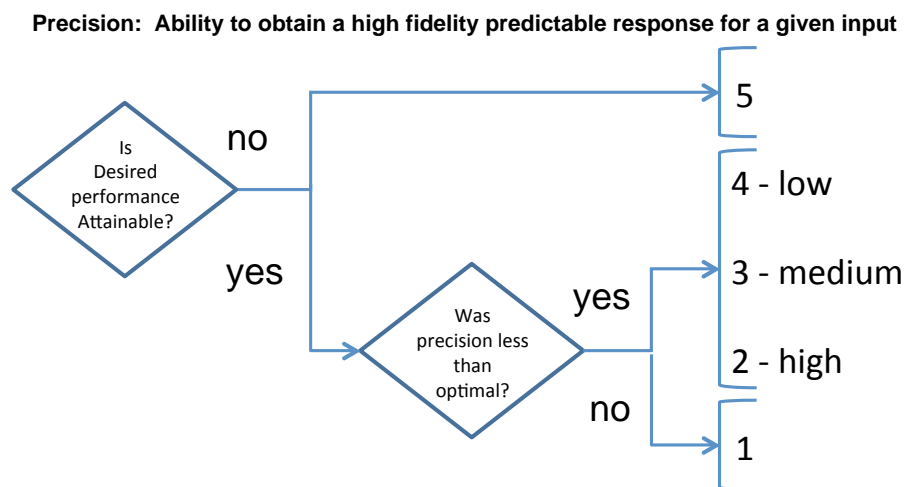
|             |               |
|-------------|---------------|
| Predictable | Unpredictable |
| 1           | 2             |
| 3           | 4             |
| 5           | 6             |
| 7           | 8             |
| 9           |               |

### DEMANDS ON THE PILOT

10. Describe overall control strategy in performing the task (cues used, scan, etc.).
11. Describe any control compensation you had to make to account for deficiencies in the aircraft.
12. Describe any modifications you had to make to what you would consider “normal” control technique in order to make the aircraft behave the way you wanted.

### MISC.

13. Please comment on anything else that may have influenced you.



Lusardi – Mansur – Ott – Mouser questionnaire, Sept 2013

**Figure A.1. Precision Rating Scale.<sup>16</sup>**

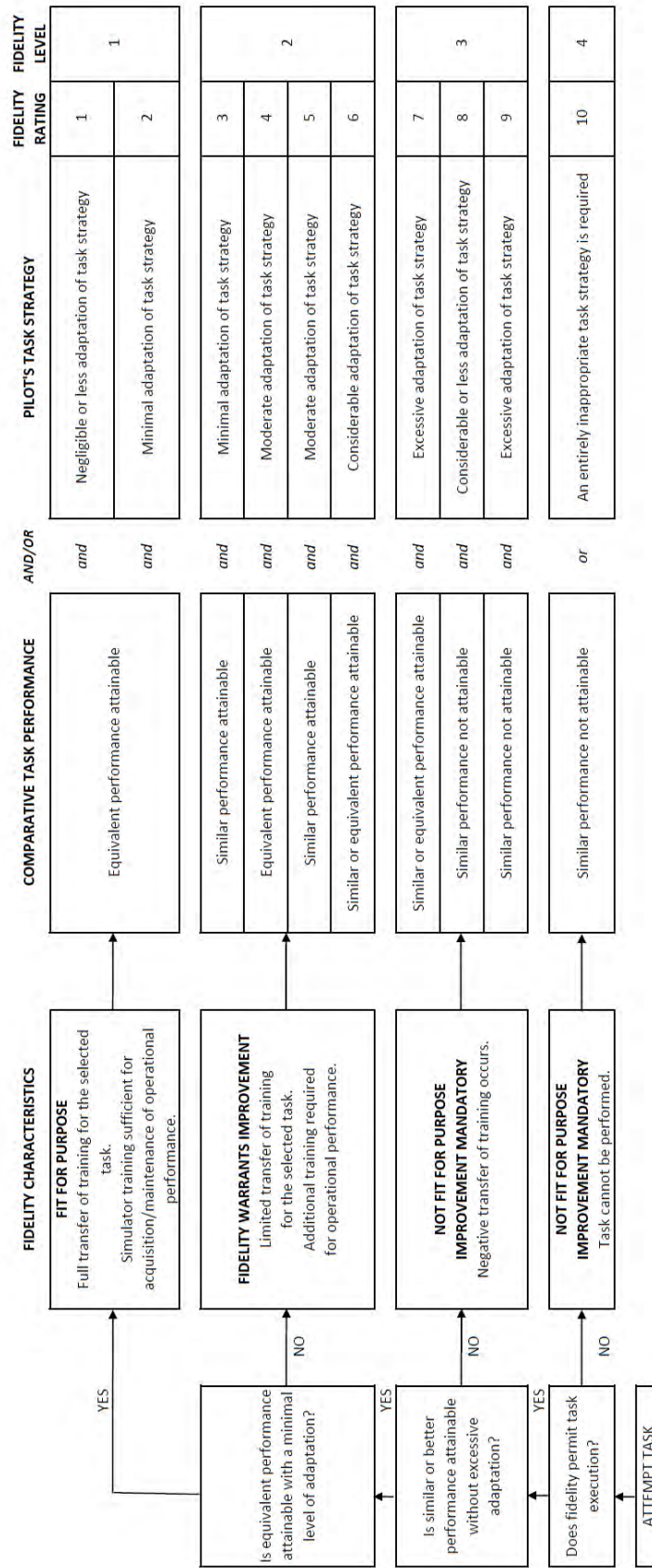


Figure A.2. Simulation Fidelity Rating (SFR) Scale.<sup>3</sup>

## Acknowledgments

The authors would like to thank the evaluation pilots, Peter Fisher and Jason Rew, and project pilot Corey Eckhart for their hard work, valuable feedback, and insightful comments. Special thanks to Jim Hammer for his efforts in integrating essential simulation hardware.

## References

- <sup>1</sup>Tischler, M. B., *Aircraft and Rotorcraft System Identification: Engineering Methods with Flight Test Examples*, American Institute of Aeronautics and Astronautics, Inc., Reston, VA, 2nd ed., 2012.
- <sup>2</sup>Roskam, J., Malaek, S., Anemaat, W., and Gerren, D., “Advanced Aircraft Analysis: A User Friendly Approach to Preliminary Design and Analysis,” *Proceedings of the AIAA Techfest XVI*, November 1989.
- <sup>3</sup>Perfect, P., Timson, E., White, M. D., Padfield, G. D., Erdos, R., Gubbels, A. W., and Berryman, A. C., “A Rating Scale for Subjective Assessment of Simulator Fidelity,” presented at the 37th European Rotorcraft Forum, Gallarate, Italy, September 2011.
- <sup>4</sup>Marcos, A. and Balas, G. J., “Development of Linear-Parameter-Varying Models for Aircraft,” *AIAA Journal of Guidance, Control, and Dynamics*, Vol. 27, No. 2, March–April 2004.
- <sup>5</sup>Aiken, E. W., “A Mathematical Representation of an Advanced Helicopter for Piloted Simulator Investigations of Control-System and Display Variations,” NASA TM 81203, AVRADCOM TM 80-A-2, July 1980.
- <sup>6</sup>Tischler, M. B., “Aerodynamic Model for Piloted V/STOL Simulation,” Systems Technology, Inc., WP 1171-2, Hawthorne, CA, May 1982.
- <sup>7</sup>Zivan, L. and Tischler, M. B., “Development of a Full Flight Envelope Helicopter Simulation Using System Identification,” *Journal of the American Helicopter Society*, Vol. 55, No. 022003, 2010, pp. 1–15.
- <sup>8</sup>Lawrence, B., Malpica, C. A., and Theodore, C. R., “The Development of a Large Civil Tiltrotor Simulation for Hover and Low-Speed Handling Qualities Investigations,” 36th European Rotorcraft Forum, Paris, France, September 2010.
- <sup>9</sup>Mansur, M. H., Tischler, M. B., Bielefeld, M. D., Bacon, J. W., Cheung, K. K., Berrios, M. G., and Rothman, K. E., “Full Flight Envelope Inner-Loop Control Law Development for the Unmanned K-MAX,” American Helicopter Society 67th Annual Forum, Virginia Beach, VA, May 2011.
- <sup>10</sup>Tobias, E. L. and Tischler, M. B., “A Model Stitching Architecture for Continuous Full Flight-Envelope Simulation of Fixed-Wing Aircraft and Rotorcraft from Discrete Point Models,” Technical Memorandum, manuscript in preparation.
- <sup>11</sup>Stevens, B. L. and Lewis, F. L., *Aircraft Simulation and Control*, John Wiley & Sons, Inc., Hoboken, NJ, 2nd ed., 2003.
- <sup>12</sup>McRuer, D., Ashkenas, I., and Graham, D., *Aircraft Dynamics and Automatic Control*, Princeton University Press, Princeton, NJ, 1973.
- <sup>13</sup>Smith, R. E. and Sarrafian, S. K., “Effect of Time Delay on Flying Qualities: An Update,” *AIAA Journal of Guidance, Control, and Dynamics*, Vol. 9, No. 5, 1986, pp. 578–584.
- <sup>14</sup>Klyde, D. H. and Mitchell, D. G., “Handling Quality Demonstration Maneuvers for Fixed-Wing Aircraft, Volume II,” WL-TR-97-3100, October 1997.
- <sup>15</sup>Cooper, G. E. and Harper, Jr., R. P., “The Use of Pilot Rating in the Evaluation of Aircraft Handling Qualities,” NASA TN D5153, April 1969.
- <sup>16</sup>Lusardi, J. A., Blanken, C. L., Ott, C. R., Malpica, C. A., and von Gruenhagen, W., “In Flight Evaluation of Active Inceptor Force-Feel Characteristics and Handling Qualities,” presented at the American Helicopter Society 68th Annual Forum, Fort Worth, TX, May 2012.